5-2023

Wave Excited Mass-Spring-Damper System for a Self-recharging Autonomous Underwater Vehicle

Mahmodul Hasan Maheen
The University of Texas Rio Grande Valley

WAVE EXCITED MASS-SPRING-DAMPER SYSTEM FOR A SELF-RECHARGING AUTONOMOUS UNDERWATER VEHICLE

A Thesis

by

MAHMODUL HASAN MAHEEN

Submitted in Partial Fulfillment of the

Requirements for the Degree of

MASTER OF SCIENCE IN ENGINEERING

Major Subject: Mechanical Engineering

The University of Texas Rio Grande Valley

May 2023

WAVE EXCITED MASS-SPRING-DAMPER SYSTEM FOR A SELF-RECHARGING AUTONOMOUS UNDERWATER VEHICLE

A Thesis
by
MAHMODUL HASAN MAHEEN

COMMITTEE MEMBERS

Dr. Yingchen Yang
Chair of Committee

Dr. Horacio Vasquez
Committee Member

Dr. Dumitru Caruntu
Committee Member

May 2023

ABSTRACT

Maheen, Mahmodul H., Wave Excited Mass-Spring-Damper System for a Self-Recharging Autonomous Underwater Vehicle. Master of Science in Engineering (MSE), May, 2023, 69 pp., 2 tables, 26 figures, references, 69 titles.

Autonomous underwater vehicles' (AUVs) endurance is constrained by the lifetime of their batteries and the distance that tether wires can traverse. Solving the endurance problem of AUV using the enormous potential of ocean wave energy is the motivation behind this thesis. The objective of this research is to model a mass-spring-damper system to emulate the permanent magnet linear generator (PMLG) of a self-recharging AUV and identify its energy absorption capability through numerical simulation and experimental testing. The research activities started with modeling and fabricating a 1:5 scale model. The scaling was done by comparing the most common AUV size of 1.5m. The preliminary dry testing result confirmed the inadequate damping of the devised prototype. After detailed wave tank testing with a fixed PTO, the vertical orientation of the converter was chosen for the second stage research. A modified 1:3 large-scale prototype was developed in the next phase. The model showed strong oscillating mass motion in the dry test rig. Comparison with numerical simulation showed that for lower wave frequency, the damping coefficient of the model matches well with the experimental result. But the prototype damping behavior is much more complex for a higher wave frequency. The tank testing confirmed that the prototype pitch amplitude in the wave needs to be enhanced for higher energy absorption.

DEDICATION

First, I want to thank almighty Allah for giving me the strength to accomplish the thesis and bringing me closer during the journey. I am also grateful to my parents and my siblings for always believing in me and giving me good wishes. It would not have been possible without their support. Finally, my deepest love for the person who has been by my side throughout the ride.

Thank you very much!

ACKNOWLEDGMENTS

This thesis would not have been successful without the generous support of many people. First and foremost, my sincere gratitude to Dr. Yingchen Yang for his constant supervision and guideline to do this research. I was lucky to trust him whenever I face any difficulties with my research. I am also indebted to Mr. Antonio Suarez for helping me with the machining of my prototype. I have learned a lot from him while working in the Brownsville machine shop. Finally, I would like to thank the Presidential Graduate Research Assistantship (PGRA) program of UTRGV for supporting me financially during my Master's.

TABLE OF CONTENTS

Page

ABSTRACT iii
DEDICATION iv
ACKNOWLEDGMENTS v
TABLE OF CONTENTS vi
LIST OF TABLES viii
LIST OF FIGURES ix
CHAPTER I. INTRODUCTION 1
Environmental Threats, World Energy Scenario, and Renewable Energy 1
Ocean Wave Energy 3
The History and Development of Wave Energy Conversion 4
Wave Energy Converter (WEC) Classifications 5
Wave Energy Engineering Challenges 5
Ocean Robotics and Marine Renewable Energy 7
Motivation 10
Objectives and Methodologies 11
CHAPTER II. CONCEPT DESIGN 13
Description of the Concept Model 13
Mathematical Modeling of the PTO Motion in AUV 15
Vertical orientation 15
Horizontal orientation 18
CHAPTER III. ANALYSIS OF A SMALL-SCALE PTO MODEL 20
3D Modeling of the Designed 1:5 Scale PTO system 20
The Physical Model and Prototype Configurations 21
Experimental Campaign 23

Dry Test: The Wave Simulation Rig 23
Wave Flume and the Wave Maker....25
Experimental observations for Fixed Power Take-off....26
Analysis of the converter behavior in the vertical orientation....26
Analysis of the converter behavior in the horizontal orientation....29
Numerical Modeling 31
Numerical Modeling Strategy....31
Numerical Simulation Result....33
Vertical orientation 33
Horizontal orientation 42
Result Analysis 49
CHAPTER IV. ANALYSIS OF A BIG-SCALE PTO MODEL....51
3D Modeling of the Designed 1:3 Scale PTO System.... 51
The Physical Model and Prototype Configurations....52
Dry Test of the 1:3 Scaled Model.... 54
Numerical Simulation of the 1:3 Scaled Model.... 56
Analysis of the Dry Test and Numerical Simulation.... 57
Wave Tank Testing....59
CHAPTER V. CONCLUSION AND FUTURE WORK 62
REFERENCES 64
BIOGRAPHICAL SKETCH 69

LIST OF TABLES

Page

Table 1: Simulation Parameters for the 1:5 Scaled Model 33
Table 2: Simulation Parameters for the 1:5 Scaled Model 57

LIST OF FIGURES

Page

Figure 1: The resemblance of global energy demand and carbon emissions 2

Figure 2: Global annual mean wave power estimation.....3

Figure 3: Marine renewable energy powered AUVs 8

Figure 4: Cutaway view of a wave powered AUV concept.....13

Figure 5: AUV (a) cruising mode and (b, c, or d) recharging mode.....14

Figure 6: (a, b) definition of parameters and (c) AUV in a vertically static equilibrium 16

Figure 7: Definition of parameters in a horizontal static equilibrium 19

Figure 8: 3D model of the 1:5 scaled sealed PTO system 21

Figure 9: 1:5 scaled model; (a) PTO masses, (b) damper house, (c) hull end, (d) screws with different diameter holes, (e) damper rod, and (f) the assembled model 22

Figure 10: (a) 3D model, and (b) physical model of the experimental rig 24

Figure 11: (a) Wave tank facility; (b) single flap type wave maker 25

Figure 12: PTO fixed AUV motion in wave frequency 0.5 Hz and height 0.113 m. Here, T means the wave period.....27

Figure 13: PTO fixed AUV motion in wave frequency 0.7 Hz and height 0.242 m. Here, T means the wave period.....28

Figure 14: PTO fixed AUV motion in wave frequency 0.5 Hz and height 0.113 m. Here, T means the wave period.....29

Figure 15: PTO fixed AUV motion in wave frequency 0.7 Hz and height 0.242 m. Here, T means the wave period.....30

Figure 16: Power curves; (a) wave of frequency 0.3 Hz and height 0.137 m, (b) wave of frequency 0.5 Hz and height 0.113 m, (c) wave of frequency 0.6 Hz and height 0.198 m, and (d) wave of frequency 0.7 Hz and height 0.242 m 35

Figure 17: Position-velocity-time plots for a wave of frequency 0.5 Hz and height 0.113 m.....41

Figure 18: Power curves; (a) wave of frequency 0.3 Hz and height 0.137 m, (b) wave of frequency 0.5 Hz and height 0.113 m, (c) wave of frequency 0.6 Hz and height 0.198 m, and (d) wave of frequency 0.7 Hz and height 0.242 m 43

Figure 19: Position-velocity-time plots for a wave of frequency 0.5 Hz and height 0.113 m.....48

Figure 20: 3D model of the 1:3 scaled sealed PTO system 52

Figure 21: 1:3 scaled model; (a) PTO mass, (b) damper house, (c) outer hull, (d) the assembled model.....53

Figure 22: 1:3 scaled prototype model mounted on experimental dry test rig 54

Figure 23: Frequency and mass translation for; (a) different air hole diameters, and (b) different AUV amplitude 55

Figure 24: Frequency and mass translation for; (a) 60, and (b) 90 Degrees of AUV angular amplitude 58

Figure 25: AUV motion in wave frequency 0.5 Hz and height 0.113 m. Here, T means the wave period 58

Figure 26: (a) 3D model of the PTO system, (b) physical model of the PTO system in wave tank, and (c) sealed PTO system with attached fins 61

CHAPTER I

INTRODUCTION

Environment Threats, World Energy Scenario, and Renewable Energy

Thomas Robert Malthus, Charles Fourier, Mary Shelley, and John Stuart Mill were among the great thinkers who made astounding predictions in the early 19th century about the impending depletion of fossil fuel resources due to industrialization and population growth (Dresner, 2002). Energy is the primary force behind the information and technology revolution of the twenty-first century and is a clear indicator of a nation's development and advancement. The average global energy consumption per capita worldwide in 2020 was 159.1 GJ in OECD nations, followed by 125.2 GJ in European Union nations and 52.8 GJ in non-OECD countries (BP, 2021). The electricity demand in 2040 is projected to be more than 40% of global energy consumption from today (Colton, 2013). Traditional energy sources such as coal, petroleum, and natural gas will not be able to meet such high demand (Zhang et al., 2021). Access to affordable and clean energy by 2030 is the seventh goal in the 17 United Nations Sustainable Development Goals list, but approximately one billion people still live without electricity (IEA et al., 2020). In addition, fossil fuels are mostly to blame for carbon emissions and are projected to push global warming up by 1.5 degrees between 2030 and 2052 (UN, 2015; IEA, 2020), which would threaten the Paris Climate Change Agreement and UN sustainable development targets.

A startling fact is that the energy sector's cumulative worldwide carbon emissions over the last 27 years match the total for all prior years, with fossil fuels accounting for more than 80% of the principal energy mix (IEA, 2015). Undoubtedly, the effects of human activity on the environment, the energy problem, and sustainability are critical issues for many nations and organizations (EC, 2019; Mayer, 2019). But there is hope, thanks to the availability of clean and

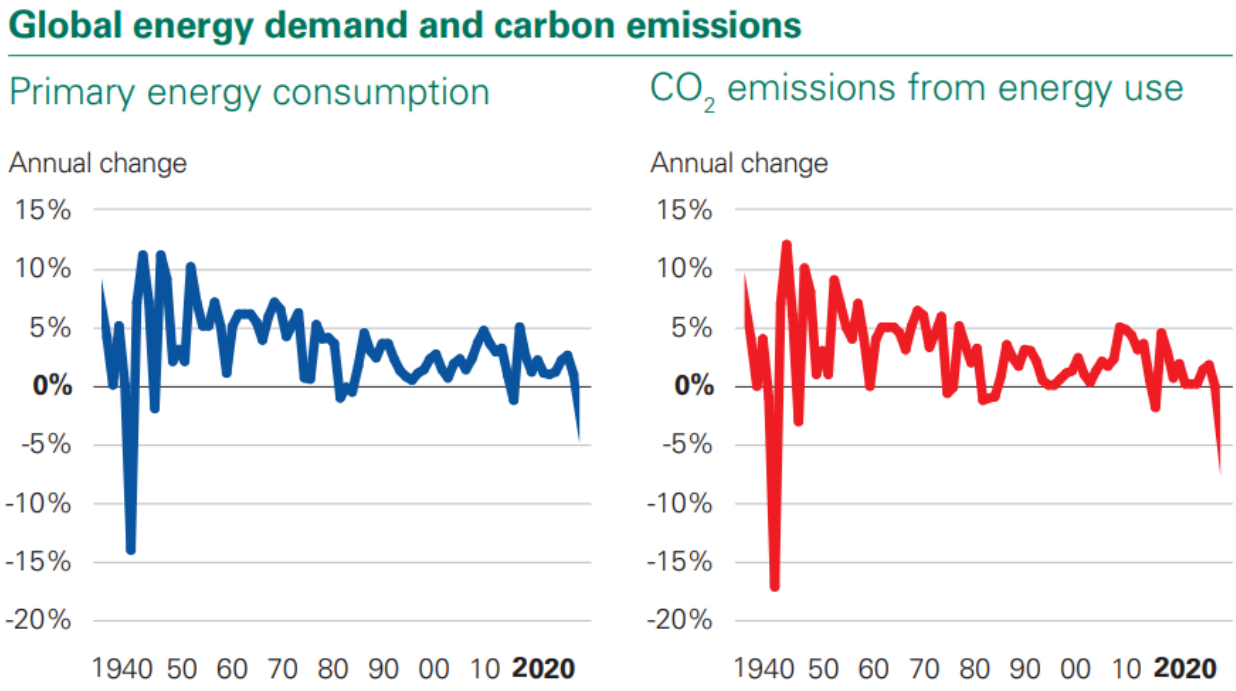

Fig. 1. The resemblance of global energy demand and carbon emissions (BP, 2021).

renewable energy sources, including solar, wind, hydropower, biomass, and geothermal resources. Solar and wind energy have shown tremendous potential recently. For instance, in 2020, renewable energy saw its highest-ever growth of 358 TWh, primarily from wind and solar energies (BP, 2021). Aside from this, there is a renewable energy source that belong to the ocean and is still largely untapped. We will talk about it in the next section.

Ocean Wave Energy

Marine renewable energy is an abundant renewable energy source that is untapped and has an estimated power of about 151,300 TWh/yr (Taveira-Pinto et al., 2015). It comprises ocean currents, thermals, waves, tides, and salinity gradients. With a technical potential of roughly 5,600 TWh/yr, ocean waves have the second-highest theoretical potential, coming in at 32,000 TWh/yr just behind ocean thermal (Edenhofer et al., 2012; Ilyas et al., 2014). Globally and in various regions, wave power assessments have been made, for example, in the coastal waters of Mexico (Hernandez-Sanchez et al., 2021), the Persian Gulf (Goharnejad et al., 2021), Latin America and Europe (Basañez & Pérez-Muñuzuri, 2021), China (Xu et al., 2021), the United States (Ahn et al., 2021), and more. Compared to solar and wind power, wave power is significantly denser, more

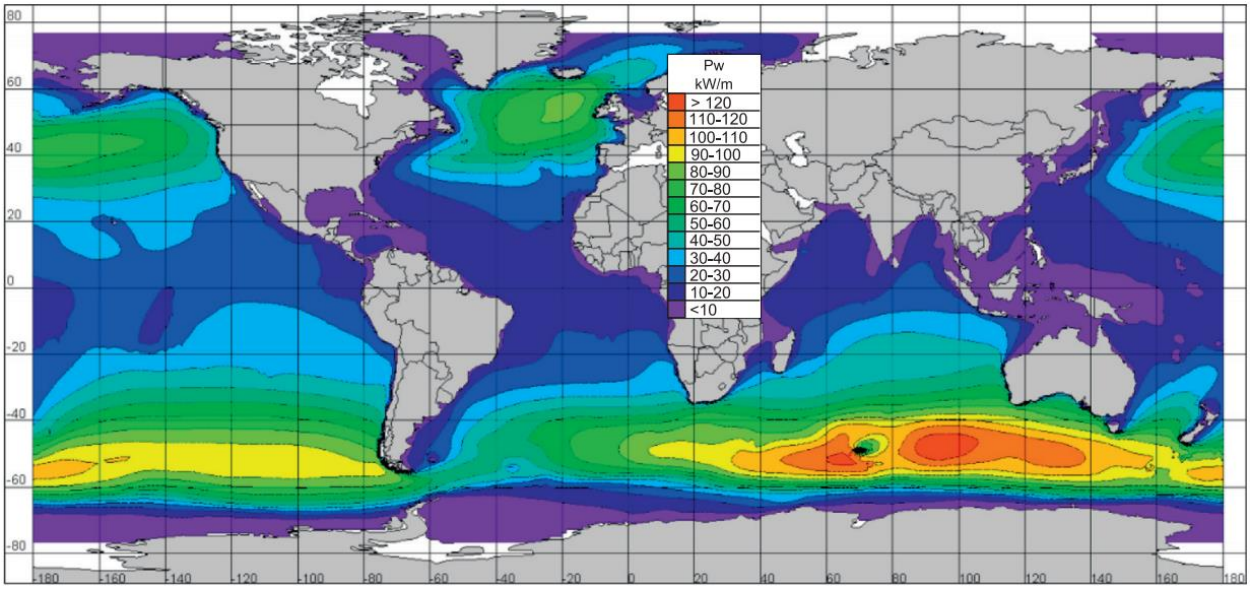

Fig. 2. Global annual mean wave power estimation (López et al., 2013).

reliable, and more stable (Pelc & Fujita, 2002; Cruz, 2008). Wave energy has potential applications in big-scale grid-connected power generation, marine buoys, and lighthouses. It can also be used

for a distributed generation because 40% of the world's population lives along coastlines (UN, 2017).

The History and Development of Wave Energy Conversion

A wave energy converter (WEC) is a device that uses energy from ocean waves to generate electricity. Girard and his son were the first to obtain a patent on WEC in France in 1799 (Clément et al., 2002). Yoshio Masuda, a Japanese marine captain who created a floating oscillating water column device for navigation buoys, conducted the first known WEC study in the 1940s (Masuda, 1986). In the 1970s, crude oil prices skyrocketed due to restrictions on Middle Eastern oil supply. This led to the beginning of some academic research on WECs in both Europe and the United States (Lindquist, 2017; Salter, 1974). Two groundbreaking papers were published in Nature magazine, one of which was written by Stephen Salter of the University of Edinburgh. Salter proposed the Salter Duck, which has become a well-known design. The other publication came from the Norwegian Institute of Technology's Budar and Falnes (Budar & Falnes, 1975), who coined the term "point absorber" to describe objects having horizontal dimensions much smaller than the wavelength. Michael E. McCormick was a pioneering academic wave-power researcher in the USA. In the 1980s, the oil price fell again, and the research gradually stopped due to a lack of funding. Early research mainly concentrated on hydrodynamic studies, the creation of oscillating water column WECs and point absorber WECs, and theoretical work to advance our fundamental understanding of ocean wave energy. As a result of the current rise in energy demand and climate change, wave energy research has been revitalized and has remained strong ever since. More than 1,000 WEC designs have been proposed globally, some of which have been prototyped

for testing in labs or open water in preparation for commercialization (Pelc & Fujita, 2002; Czech & Bauer, 2012).

Wave Energy Converter (WEC) Classifications

Wave Energy Converters (WECs) can be categorized based on several factors. According to working principles, there are five types of WECs: oscillating water column, overtopping, oscillating body, pressure differential, and impact (Falcão, 2010; López et al., 2013). There are onshore, nearshore, and offshore WECs based on deployment locations (López et al., 2013). There are three types of WECs: attenuator, point absorber, and terminator depending on the size and orientation of a device about incoming waves (López et al., 2013; Czech & Bauer, 2012). There are reciprocating and unidirectional WECs depending on the direct wave-enabled motion type (Yang et al., 2020; Ermakov & Ringwood, 2021). Classifications based on power take-off (PTO) include mechanical, hydraulic, pneumatic, and directly electrical systems (Falnes, 2007). The European Marine Energy Center divided WECs into eight major kinds for a more thorough identification (EMEC, 2022).

Wave Energy Engineering Challenges

In contrast to the enormous potential of wave energy and the wide range of WEC concepts, practical WEC advancements for field deployment still lag behind solar and wind energies in terms of technological maturity (IRENA, 2014; Aderinto & Li, 2018). Failure to achieve technical convergence (Topper et al., 2019; Pecher & Kofoed, 2017), high levelized cost of energy (Astariz & Iglesias, 2015; Astariz & Iglesias, 2016), and hostile ocean environment (Borthwick, 2016; Tiron et al., 2015) are some crucial factors behind this. Besides, a slow, unpredictable, and

oscillating wave motion needs to be transformed into electricity that can be integrated into the grid by employing the right electromagnetic generator and increasing the generated voltage level in order for a WEC technology to be commercially viable (López et al., 2013; Czech & Bauer, 2012).

A WEC's ability to operate successfully requires that it endures in harsh maritime conditions for more than 20 years (Tiron et al., 2015). Oceans are continuously undergoing diverse biological, chemical, and physical transformations. Hence, the devices will experience biofouling and corrosion (Tiron et al., 2015). As the WECs serve as artificial reefs for the growth of algae and the habitation of marine animals, biological activity like the growth of mollusks and seaweed, the formation of bacterial biofilms, and fish movement provide extra obstacles. Such actions increase the masses on the WECs and restrict the mobility of various section, which lowers the WEC efficiency (Tiron et al., 2012; Inger et al., 2009). Furthermore, the colonization of marine species results in anoxic and low pH conditions that exacerbate the need for operational part replacement and maintenance (Tiron et al., 2015).

The maintenance requirements for offshore WECs are accelerated by extreme wave conditions such as storms and rogue waves (Nikolkina & Didenkulova, 2011; O'Brien et al., 2013). Large storm waves are frequently seen in high-energy-density areas, which could be used for WEC deployment. For nearshore and shoreline WECs, threats from tsunamis, storm surges, and breaking waves are also typically present. These wave conditions result in highly nonlinear hydrodynamic forces (Henry et al., 2014). Designing for increased survivability could lower WEC efficiency. Therefore, for a successful WEC technology, there needs to be a balance between these two opposed factors. Additionally, a long and uninterrupted period of calm sea conditions is preferred

for WEC deployment and maintenance. But the active wave farm sites typically have extremely brief undisturbed weather intervals (Tiron et al., 2015). It is estimated that annual operation and maintenance costs of ocean energy devices can be as high as about 3.4–5.8% of capital expenditure compared to 2.3– 3.7% for offshore wind (Lacal-Arantegui et al., 2014). For each of these reasons, WEC designs that are simple to deploy and need less maintenance would be greatly appreciated (Mueller & Wallace, 2008; Uihlein & Magagna, 2016).

Ocean Robotics and Marine Renewable Energy

Ocean robots have been regarded as one of the crucial tools for understanding and exploring the ocean, especially in harsh underwater high-pressure environments. Unmanned marine robots possess specialized intelligence. Unmanned surface vehicles (USVs) and unmanned underwater vehicles (UUVs) are the two main categories for these gadgets. The UUVs can also be divided into autonomous underwater vehicles (AUVs) and remotely controlled vehicles (ROVs). While ROVs are guided by an operator via a tethered cable when operating, AUVs carry out operations like sensing and autonomous decision-making without human supervision (Roberts & Sutton, 2006). AUVs are used for several purposes, including surveillance, research, and commercial applications.

The autonomy of AUVs depends on two things: the number of hours they can operate without help and their decision-making autonomy (Aguirre et al., 2017). The power source determines how long ocean robots can run. Batteries and tether power systems have been the primary power sources for maritime robots thus far. They do, however, have their limits. Because batteries only last so long, a docking device is required for continued use. Tethered cables make it

difficult for a vehicle to move farther. In these UUVs, the necessary endurance and finite energy issues can be resolved by using the enormous marine renewable energy (MRE) as an alternate source. Ocean robots powered by MRE are now starting to appear in considerable numbers and are being used for numerous purposes. We will now briefly go over the AUVs powered by renewable energy.

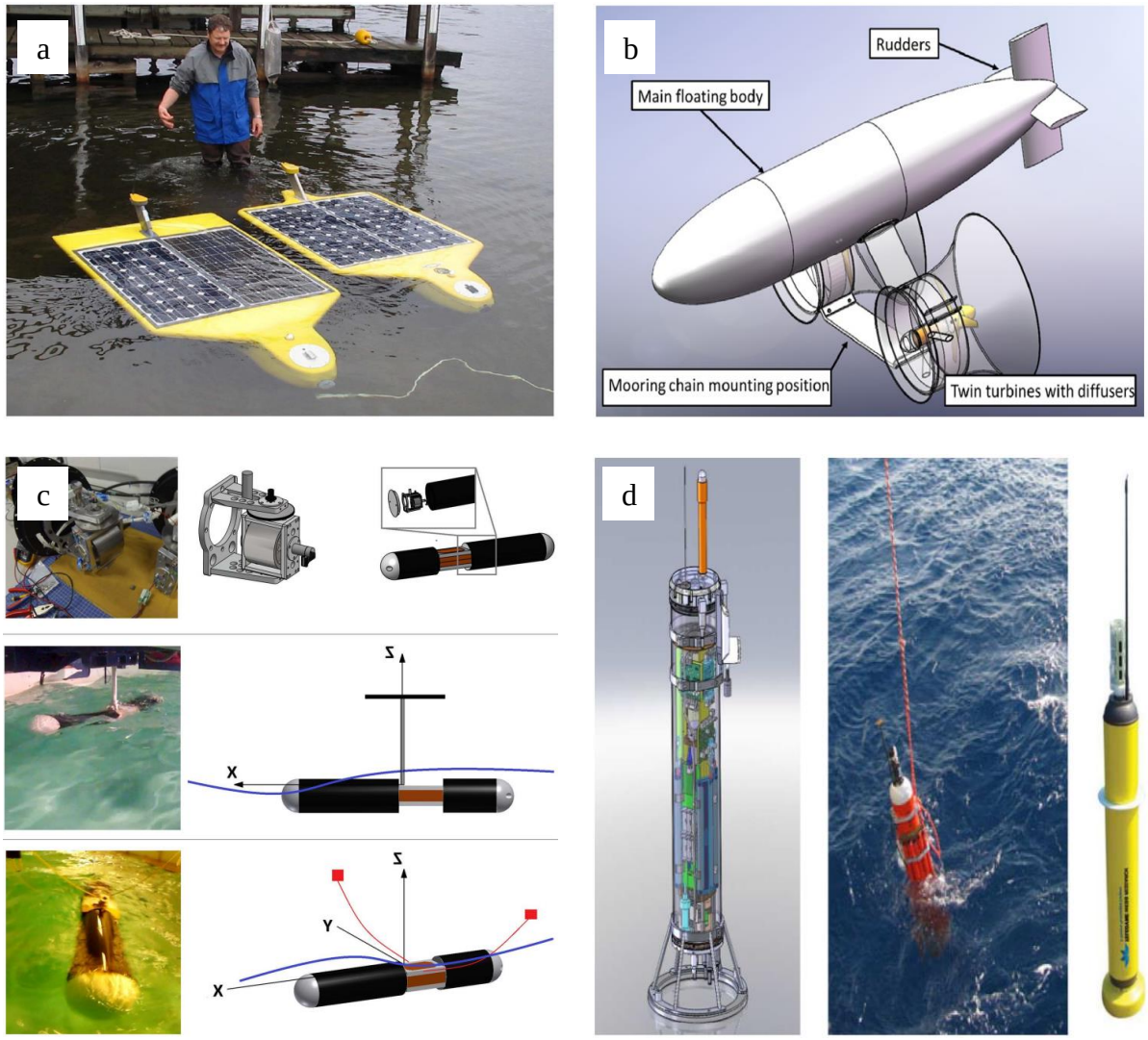

Fig. 3. Marine renewable energy powered AUVs; (a) solar-powered AUV SAUV-II, (b) tidal current powered AUV, (c) wave energy powered AUV, and (d) thermal energy powered SOLO-TREC (Komerska & Chappell, 2006; Shi et al., 2015; Townsend, 2016; Smith & Huynh, 2014).

The Autonomous Undersea Systems Institute (AUSI) and the Institute for Marine Technology Problems of the Russian Academy of Sciences jointly produced an engineering prototype solar-powered AUV named SAUV I. The 22-day successful sea trial near Vladivostok attested to the SAUV I's durability (Ageev & Blidberg, 2002). Based on the success, AUSI created the SAUV II, which has a speed range of 0.75 to 3 knots, in collaboration with Technology Systems Inc. and Falmouth Scientific Inc. (Komerska & Chappell, 2006; Blidberg et al., 2005; Jalbert et al., 2004). The new AUV's performance and endurance were significantly enhanced (Crimmins et al., 2006). In 2004, several field experiments based on SAUV II were conducted in Lake George and Greenwich Bay regarding the communication between numerous units (Blidberg et al., 2005). However, due to the restricted availability of sunlight and its poor power density, SAUV-II must use the entire day for recharging and only the night for missions. Biofouling has a significant impact on SAUV-II recharging as well.

To increase the durability of AUVs, Newcastle University presented a revolutionary idea driven by tidal currents (Shi et al., 2015). The AUV contained three subsystems. To generate electricity, a pair of twin diffuser-augmented tidal turbines were installed. Researchers from NASA's Jet Propulsion Laboratory, Scripps Institution of Oceanography, and the University of California developed the SOLO-TREC, a robotic underwater vehicle powered by thermal energy (Smith & Huynh, 2014). When the AUV crosses the thermocline—the boundary between warm surface water and chilly deep water—it absorbs thermal energy. The absorbed thermal energy is converted to electricity by a unique thermal engine, which recharges the batteries.

Although there have been several approaches to incorporating marine renewable sources into AUVs, they have faced some critical issues. Solar power is only available during the day, and

the density is also very low. Ocean currents and ocean thermal do not have adequate power production capacity to run the AUVs. Wave energy as an ocean robot power source offers tremendous promise. However, there has not been enough research to exploit this source.

Townsend et al. from the University of Southampton have presented a unique gyroscopic wave energy conversion device for AUVs. Based on the control moment gyroscope principle, the gyroscopic response of a gimballed flywheel was employed to convert the wave energy to electricity. The wave motion stimulates the flywheel's rotational action (Townsend & Shenoi, 2016). To generate more power, future research must regulate the PTO and reduce its friction (Townsend & Shenoi, 2016).

Motivation

I am a citizen of Bangladesh, one of the ten countries most affected by global warming this century, and a country that is expected to lose 11% of its land by 2050 due to the sea-level rise, according to The New York Times. I have always felt the necessity for clean and sustainable energy sources. Ocean wave energy can deal with these concerns because of its massive untapped potential. In addition, it can be an alternative power source for marine robotics. Ocean robots have been considered one of the crucial tools for exploring and comprehending the ocean, particularly in remote and dangerous places. The limited duration of batteries and the travel constraint of tether cables shorten the endurance of these robots. My motivation is to incorporate ocean wave power into the current energy portfolio and make it suitable for autonomous underwater vehicles (AUVs).

An autonomous underwater vehicle (AUV) fueled by wave energy will prolong its endurance and forward presence as there is no logistic tail for fuel. The AUV will always have

access to a sustainable energy source because of the constant wave energy flow. The batteries can be made lighter, which will allow additional sensor applications. These two benefits make the ocean waves an excellent choice for self-recharging the AUVs. However, a wave energy harvesting device with a small size and high output is required for a compact AUV design. Unfortunately, this kind of strategy has yet to be shown effective.

Wave energy converter (WEC) technologies have been investigated recently to generate power on a utility scale (Falcão, 2010; Sheng, 2019; Shami et al., 2018). However, most of them cannot be applied to AUV applications simply because their operating circumstances do not match those of AUVs. Also, to protect the mechanical components and electric sensors from the corrosive effects of seawater, the PTO system of wave energy converters should be encased inside the hull of the AUV. In this circumstance, a spar-shaped reciprocating WEC with a fully hull-encapsulated mass-spring-damper system for power takeoff (PTO) merits special consideration (Grilli et al., 2007; Chen et al., 2018; Gao et al., 2016). The PMLG, with its enormous capacity and excellent efficiency, can be used as the PTO system because of very few conversion stages. It is a perfect fit for powering autonomous underwater vehicles because it often has small, portable designs that are especially suitable for reciprocating WECs. Moreover, to make the technologies self-sufficient, advanced, and competitive, the energy harvesting cost should be drastically decreased.

Objectives & Methodologies

The objective of this thesis is to:

- Design and fabricate the permanent magnet linear generator (PMLG) power take-off (PTO) as a mass-spring-damper system

- Develop a numerical method to simulate the oscillating mass motion of the mass-spring-damper system
- Identify the control parameters for maximum power absorption
- Buy compression and expansion springs with appropriate spring constants for the fabricated physical model
- Perform dry testing and compare the dry testing data with numerical simulation to identify the damping constants of the physical model
- Calculate the wave power absorption capability of the physical model from wave tank testing

CHAPTER II

CONCEPT DESIGN

Description of the Concept Model

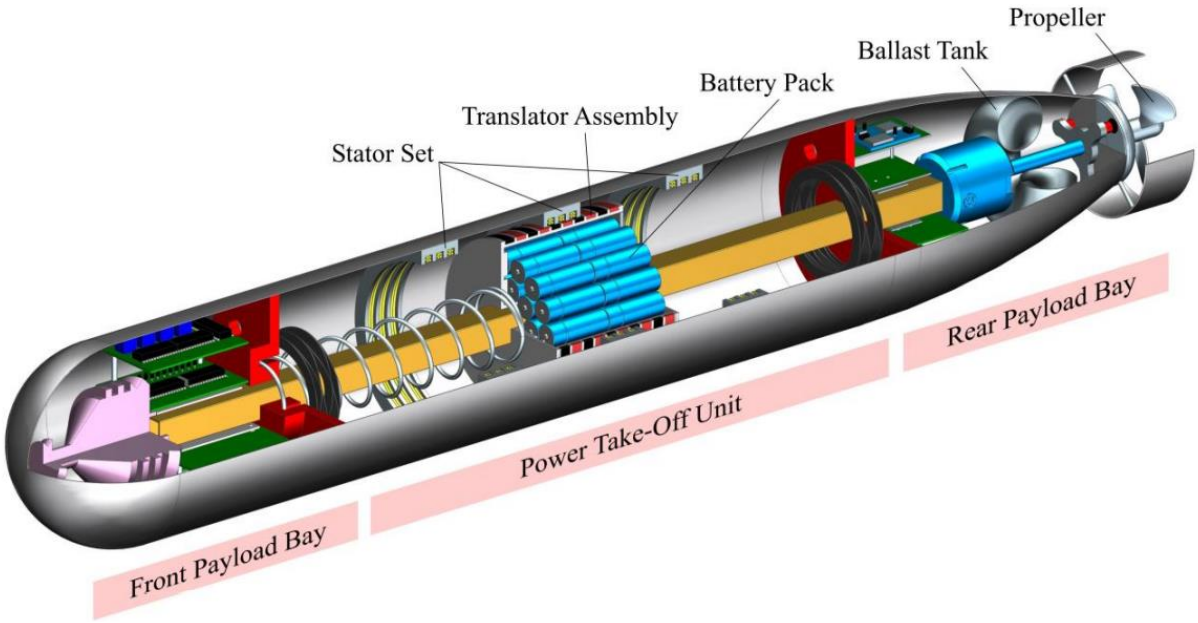

Fig. 4: Cutaway view of a wave powered AUV concept (Yang & Martinez, 2023).

The 3D design of a complete wave-powered AUV concept is illustrated in Fig. 4 (Yang & Martinez, 2023). The AUV has the most popular torpedo shape watertight rigid hull. Inside the hull, the AUV has a front and a rear payload bay for sensors and instruments necessary for the mission. It also has a mass-spring-damper PTO unit in the middle for self-recharging, a ballast tank for buoyancy control, and a propulsion unit towards the trailing end. The PTO unit comprises a spiral-shaped compression spring, two-disc springs, a translator, and a set of stators.

In waves, the AUV performs reciprocating motions such as heave, pitch, etc. With the reciprocating motion, the translator oscillates along a smooth guide rail inside the stator set facilitated by the compression spring. The relative movement between the translator and the stator set leads to electricity generation. The two high-stiffness disc springs at the two-stroke end work as an end constraint. They are also convenient for frequency-up conversion. The rechargeable battery pack embedded in the translator can add to the sliding mass and save space in the AUVs. This will increase the efficiency of the design.

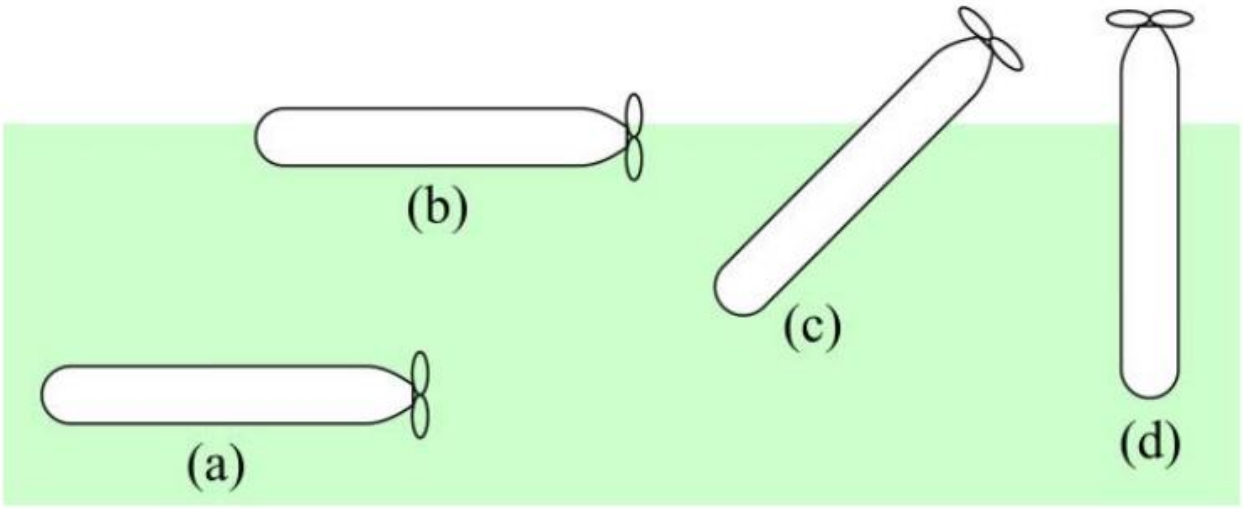

Fig. 5: (a) cruising mode and (b, c, or d) recharging mode. (Yang & Martinez, 2023).

There will be two modes for the AUV. Underwater cruising mode for mission completion and recharging mode by riding surface waves. In Fig. 5, the two approaches are illustrated. The AUV remains in a horizontal orientation and near neutral buoyancy for underwater forward cruising mode (Fig. 5a). However, when recharging, the AUV will come to the calm sea surface by active ballast control and stay in one out of three typical equilibrium orientations – horizontal (Fig. 5b), inclined (Fig. 5c), and vertical (Fig. 5d). The position of the ballast tank needs to be tuned inside the AUV to achieve the desired orientation. A vertical equilibrium orientation can be

obtained by positioning the ballast tank in the location, as shown in Fig. 4. For horizontal equilibrium orientation, the wave propagation direction and the AUV longitudinal axis need to be aligned. But it is unlikely that a torpedo-shaped powered-off AUV freely floating on the ocean surface will align and maintain its orientation with the waves. Passive control using a long fin may help get the alignment, but it will negatively affect the AUV hydrodynamic in cruising mode. On the other hand, there would be no such alignment issues for vertical orientation.

Mathematical Modeling of the PTO Motion in AUV

In this section, the PTO of the wave-powered AUV is mathematically designed as a mass-spring-damper system. The sliding mass is connected with a spring and a damper on each side to achieve a horizontal orientation. For vertical orientation, the sliding mass has a spring only on the bottom and a damper on each side. First, we will consider an AUV with a vertical equilibrium orientation and later a horizontal AUV orientation.

Vertical orientation

A fully submerged AUV's body motion in vertical equilibrium orientation would have both the heave and pitch oscillation. However, the pitch motion contribution is expected to be much more than the heave motion (Evans, 1976; Falnes, 1993). In this mathematical modeling, simple deep waves of a frequency, f_W and height, H are considered. Although the waves are simple, the AUV body motion in these waves are quite complex. This complex AUV movement is decomposed into two dominant components. Some approximations are considered to deal with wave-AUV interaction and avoid complexities. The considered motion components in waves are the orbital translation of the AUV along a circular path of diameter equal to wave height and

sinusoidal angular oscillation due to pitch motion. The pitch motion, illustrated in Fig. 6, can be expressed analytically as $\theta_{AUV} = \theta_0 sin\,(2\pi f_W t + \phi_0)$, where θ_{AUV} is the angular position, θ_0 the angular amplitude, t the time, and ϕ_0 the initial phase angle. The phase angle of sinusoidal waves $\phi = 2\pi f_W t$ is represented with respect to a vertical line.

For the analytical modeling, we will only focus on the translator's sliding motion inside the AUV. The definition of the translator's longitudinal position Z_{PTO} with respect to the AUV hull and the maximum oscillation range $2z_0$ is given in Fig. 6. In our analysis, Z_{PTO} is measured from the midpoint of the range $2z_0$. When $|Z_{PTO}| \leq z_0$, only the compression spring of stiffness k_{PTO} is active. However, both the compression spring and the disc spring jointly come into effect

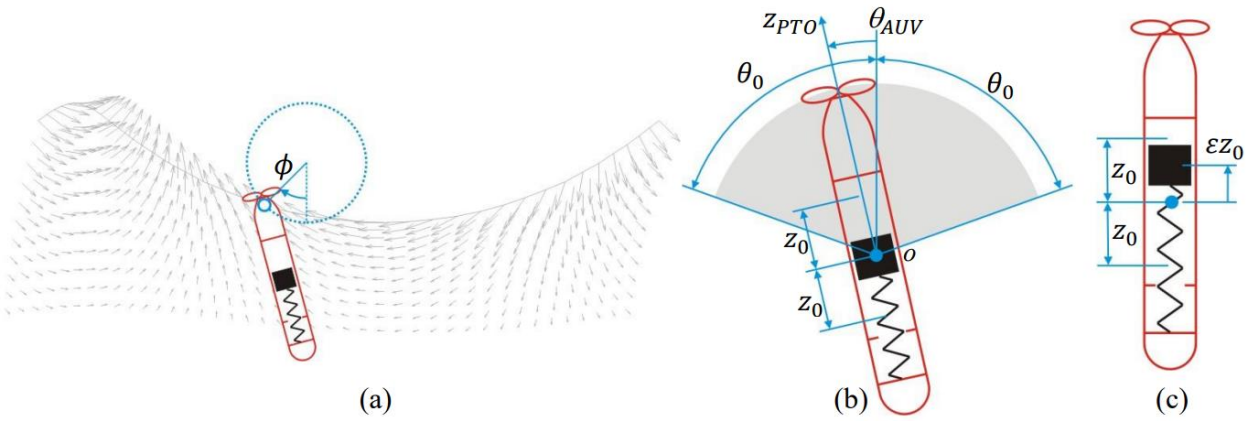

Fig. 6: (a, b) definition of parameters and (c) AUV in a vertically static equilibrium.

when $|Z_{PTO}| > z_0$. For convenience, the disk spring stiffness k is expressed as $k = nmg/z_0$, where n is a number which can be tuned. The stiffness of the disk spring can be one to three orders of magnitude higher than that of the compression spring. When the AUV body is in a vertical equilibrium orientation, and the inside translator is in static equilibrium, the position of the

translator can be measured as εz_0 (Fig. 6(c)), where ε has a value between −1 and 1. The value for ε in optimal PTO design would change the translator's oscillation in the confined range $2z_0$ and subsequently, the AUV's power generation capability.

Considering all the definitions, conditions, and assumptions, governing equations for the translator's sliding motion inside the AUV with a damping coefficient c_{PTO} are derived as follows:

$$\begin{aligned} m\ddot{Z}_{PTO} + C_{PTO}\dot{Z}_{PTO} + (k_{PTO} - m(2\pi f_W \theta_0 cos(2\pi f_W t + \phi_0))^2 Z_{PTO} \\ = -2\pi^2 {f_W}^2 mHcos\big(2\pi f_W t + \theta_0 sin(2\pi f_W t + \phi_0)\big) + (1 \\ - cos(\theta_0 sin(2\pi f_W t + \phi_0)))mg + \varepsilon k_{PTO} z_0 \quad (when\ |Z_{PTO}| \\ \leq z_0); \end{aligned} \tag{1}$$

$$\begin{aligned} m\ddot{Z}_{PTO} + C_{PTO}\dot{Z}_{PTO} + (k_{PTO} + \frac{nmg}{z_0} - m(2\pi f_W \theta_0 cos(2\pi f_W t + \phi_0))^2 Z_{PTO} \\ = -2\pi^2 {f_W}^2 mHcos\big(2\pi f_W t + \theta_0 sin(2\pi f_W t + \phi_0)\big) + (1 + n \\ - cos(\theta_0 sin(2\pi f_W t + \phi_0)))mg + \varepsilon k_{PTO} z_0 \quad (when\ Z_{PTO} \\ > z_0); \end{aligned} \tag{2}$$

$$\begin{aligned} m\ddot{Z}_{PTO} + C_{PTO}\dot{Z}_{PTO} + (k_{PTO} + \frac{nmg}{z_0} - m(2\pi f_W \theta_0 cos(2\pi f_W t + \phi_0))^2 Z_{PTO} \\ = -2\pi^2 {f_W}^2 mHcos\big(2\pi f_W t + \theta_0 sin(2\pi f_W t + \phi_0)\big) + (1 - n \\ - cos(\theta_0 sin(2\pi f_W t + \phi_0)))mg + \varepsilon k_{PTO} z_0 \quad (when\ Z_{PTO} \\ < -z_0); \end{aligned} \tag{3}$$

Horizontal orientation

Considering the identical definitions, conditions, and assumptions as of vertical orientation, governing equations for the translator's sliding motion inside a fully submerged AUV in horizontal orientation with a damping coefficient C_{PTO} are derived as follows:

$$\begin{aligned} m\ddot{Z}_{PTO} + C_{PTO}\dot{Z}_{PTO} + (k_{PTO} - m(2\pi f_W \theta_0 cos(2\pi f_W t + \phi_0))^2 Z_{PTO} \\ = -2\pi^2 {f_W}^2 mHsin\big(2\pi f_W t - \theta_0 sin(2\pi f_W t + \phi_0)\big) \\ + mgsin(\theta_0 sin(2\pi f_W t + \phi_0)) \quad (when\ |Z_{PTO}| \le z_0); \end{aligned} \tag{4}$$

$$\begin{aligned} m\ddot{Z}_{PTO} + C_{PTO}\dot{Z}_{PTO} + (k_{PTO} + \frac{nmg}{z_0} - m(2\pi f_W \theta_0 cos(2\pi f_W t + \phi_0))^2 Z_{PTO} \\ = -2\pi^2 {f_W}^2 mHsin\big(2\pi f_W t - \theta_0 sin(2\pi f_W t + \phi_0)\big) \\ + mgsin(\theta_0 sin(2\pi f_W t + \phi_0)) + nmg \quad (when\ Z_{PTO} > z_0); \end{aligned} \tag{5}$$

$$\begin{aligned} m\ddot{Z}_{PTO} + C_{PTO}\dot{Z}_{PTO} + (k_{PTO} + \frac{nmg}{z_0} - m(2\pi f_W \theta_0 cos(2\pi f_W t + \phi_0))^2 Z_{PTO} \\ = -2\pi^2 {f_W}^2 mHsin\big(2\pi f_W t - \theta_0 sin(2\pi f_W t + \phi_0)\big) \\ + mg\sin\,(\theta_0 sin(2\pi f_W t + \phi_0)))mg - nmg \quad (when\ Z_{PTO} \\ < -z_0); \end{aligned} \tag{6}$$

If we can get the translator's displacement Z_{PTO} and velocity $\dot{Z}_{PTO}$ as a function of time t using the above equations, the average power $\bar{P}$ from the PTO for both vertical and horizontal orientation can be calculated using

$$\bar{P} = \frac{C_{PTO}}{T}\int_0^T (\dot{Z}_{PTO})^2 dt, \tag{7}$$

where T is the time duration for evaluation.

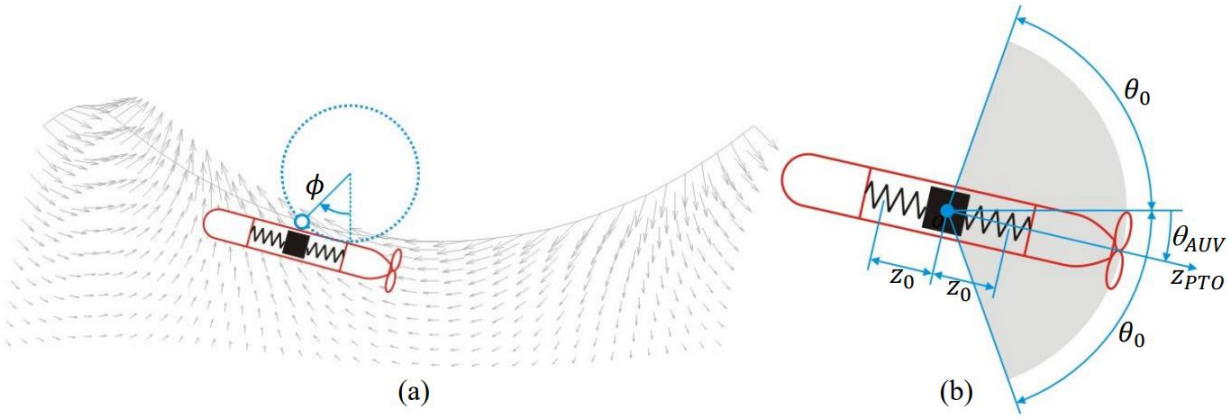

Fig. 7: Definition of parameters in a horizontal static equilibrium.

CHAPTER III

ANALYSIS OF A SMALL-SCALE PTO MODEL

Two mass-spring-damper PTO systems are designed and developed to replicate the permanent magnet linear generator (PMLG) of the self-recharged AUV in Figure 4. First, a 1:5 scaled model of a sealed PTO system was outlined. Both the 3D and physical models of this PTO system have been outlined in this chapter. After that, this small-scale PTO system's experimental testing and numerical simulation have been briefly described. Based on the results, a 1:3 scaled larger model with improvements is designed and fabricated, which will be discussed in the next chapter. The scaling of both the small and big-scale PTO systems is done by comparing the most common AUV length of 1.5 m.

3D Modeling of the Designed 1:5 Scale PTO System

The 3D model of the 1:5 scaled PTO system is shown in Figure 8. The outside hull is made of Polycarbonate round tube. The oscillating mass at the center is made of brass. Additional weights can be connected to the oscillating mass and/or the damper houses. The two damper houses are made of aluminum. The oscillating mass is press-fitted to the aluminum damper rod. The damper rod joined with the oscillating and added weights reciprocates inside the damper house and compress the air inside. This way, the system acts as a pneumatic damper. Two polycarbonate pieces were used to hold the damper houses to the hull. Oil rings have been used between the hull-

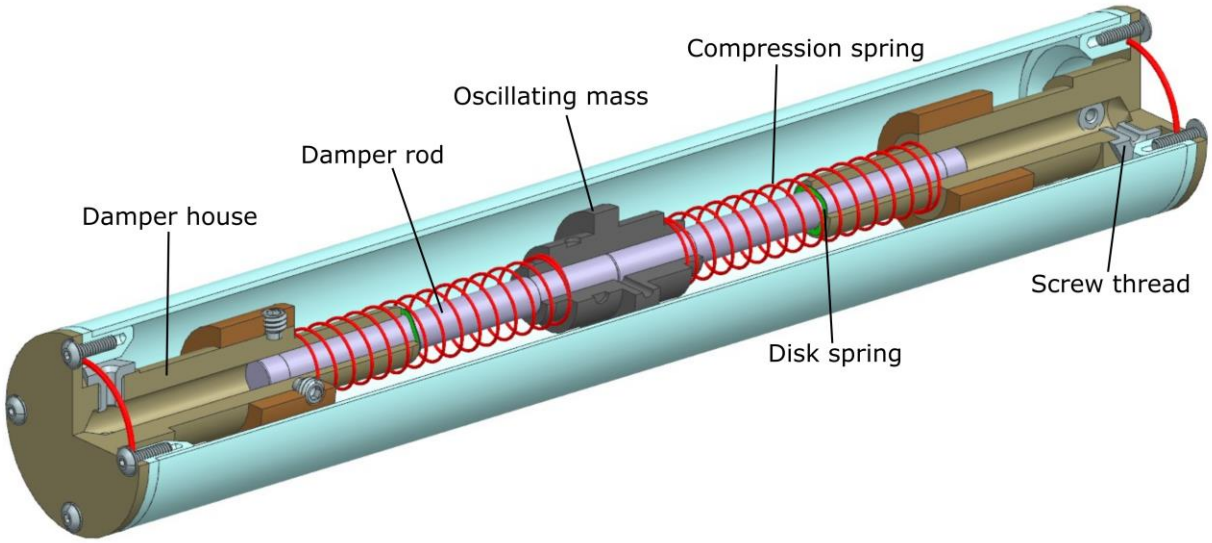

Fig. 8. 3D model of the 1:5 scaled sealed PTO system.

end and damper house to prevent water from leaking inside the system. Compression springs have been set on both sides of the oscillating mass for smooth operation. The stiffness of the springs can be varied for control purpose. At the end of the damper houses, two threads have been machined. The purpose of it is to control the damping coefficient by setting screws with appropriate diameter holes drilled into them. The forced air is blown through these holes in controlled way to act as a damping force on the oscillating mass. A disc spring has been applied at each end of the stroke for shock absorbance and frequency up-conversion. The whole system is designed to be neutrally buoyant in water.

The Physical Model and Prototype Configurations

Based on the 3D design, a 1:5 sealed PTO system was fabricated. The individual parts of the PTO system were machined in the UTRGV machine shops using appropriate machine tools by the author himself. The prototype parts were fabricated keeping in mind the dry experimental rig and wave tank testing. Several changes were made to the original 3D design depending on the

machining complexity, assembly issues, and testing requirements.

The individual parts and the total assembly of the 1:5 scaled model is shown in Figure 9.

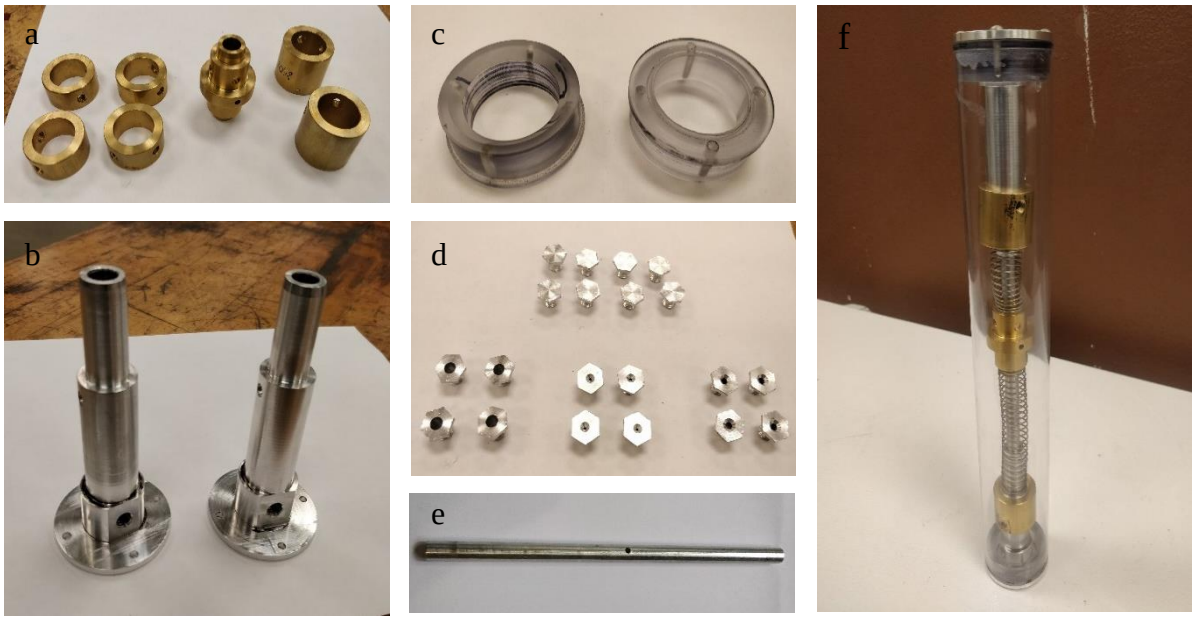

Fig. 9. 1:5 scaled model; (a) PTO masses, (b) damper house, (c) hull end, (d) screws with different diameter holes, (e) damper rod, and (f) the assembled model.

The oscillating center mass is connected to the damper rod with the help of a spring pin. In the 3D model, the damper rod is supposed to have two pieces attached to the two ends of the oscillating mass. But this causes alignment issues due to assembly difficulty. So, a single damper rod design has been opted for the physical prototype. The added masses may be mounted on the oscillating mass by screws and threaded holes. The damper rod, part of the total mass structure oscillates in the damper tube. At the hull end portion of the damper tube, there are two threaded holes on which screws of Figure 9(d) are connected. The screws have different diameter holes, which acts as a passage for the air to blow when the damper rod oscillates inside the damper tube. This way the whole structure acts as a pneumatic damper. Using different diameter holes on the screws, the air movement can be varied, which eventually controls the damping. 0.203", 0.109",

and 0.0313" diameter holes have been drilled on 12 screws, 4 screws for each diameter. At first, 8 screws were left without drilling beside the 12 drilled screws for later situation. Hull ends are glued to the hull tube using polycarbonate solvent cement. The damper tubes have been connected to the hull ends, and oil rings were used between them to prevent water leakage inside the AUV. The whole structure was neutrally buoyant. Two compression springs had been used, one on each side of the oscillating mass, which acts as an end constraint, and for smooth operation. Springs of three different stiffness have been used for this purpose.

Experimental Campaign

The experimental study is costly and lengthy. But it complements mathematical modeling and is indispensable in WEC technology development. The experimental study is done in three steps: (i) dry testing of WEC subsystems; (ii) tank, flume, and basin testing of scaled WEC models; and (iii) open water testing of scaled or full scale WEC prototypes. The purposes of experimental study include (i) proof of concept of a WEC design; (ii) performance characterization in subsystem and system levels for design optimization; and (iii) validation of mathematical models.

Dry Test: The Wave Simulation Rig

To validate the simulation results, the dynamics of the PTO were investigated on an experimental dry test rig. The rig was designed and built by the author, who also collected the data. The test rig can simulate the wave motion in real-time using a servo motor system and apply it to the PTO. In this section, the design of the experimental test rig is presented.

The 3D model and the physical manifestation of the experimental dry test rig are shown in Figure 10 (a). The PTO system is mounted on the servo motor shaft using an AUV mount, a rail,

and a connector. The servo motor was operated and controlled by a servo drive and toggle switches. A gearbox of 1:25 is attached to the servo motor shaft to reduce the speed. The servo motor can generate reciprocating sinusoidal motion of a vast frequency and amplitude range. This makes it very suitable for mass-spring-damper system testing under regular wave conditions.

Through a dry experimental test, the performance of the PTO components is assessed. In addition, the parameter choices, such as mass, spring constant, and damping coefficient of the PTO and excitation frequency and amplitude of the sinusoidal motion are explored. This is required to validate the numerical model.

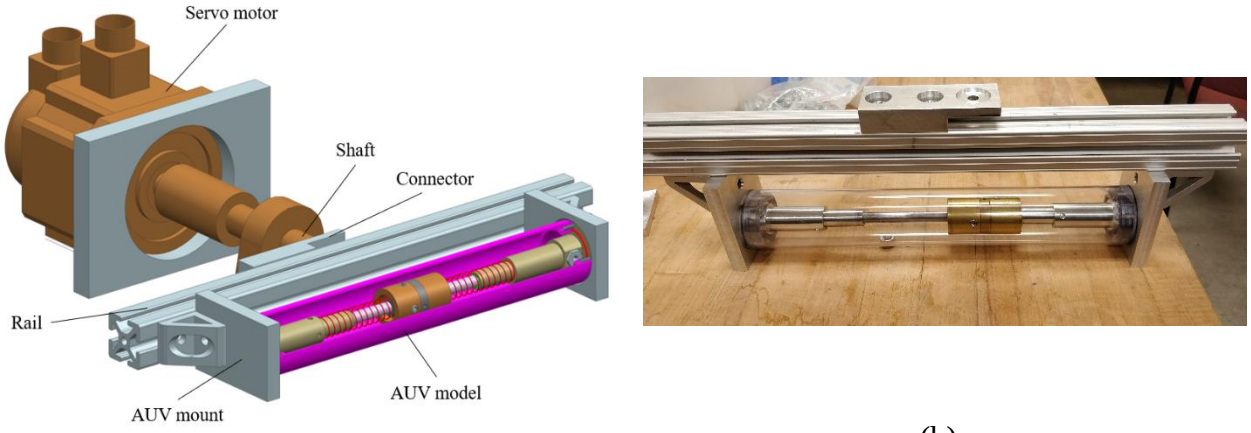

(a) (b)

Fig. 10. (a) 3D model, and (b) physical model of the experimental rig.

The most critical issue found in the preliminary dry testing of this model is the inadequate damping. Even with the smallest diameter holes drilled on the screws, which is 1/64 inch, the model did not show any significant damping. Hence, for later wave tank testing of this model, the PTO was set fixed and used to analyze the converter behavior.

Wave Flume and the Wave Maker

A crucial step in the formation of a new idea for wave energy conversion is the experimental phase in wave flumes or wave basins because it enables the identification of the important factors that affect the converter performance in a physical and controlled setting. This enables the wave energy converter to be enhanced or redesigned. Through proper scaling, the wave tank can accurately reproduce a variety of sea wave situations. A summary of the wave tank facility's dimensions and wave-maker characteristics is provided in this section.

Engineers use a variety of wave tanks to simulate sinusoidal or ocean waves in a testing setting. The testing facility's water tank is 15 meters long, 1 meter broad, and has a 1.3 meter water depth. The water tank's beach features a structure made of porous absorbing material, which can

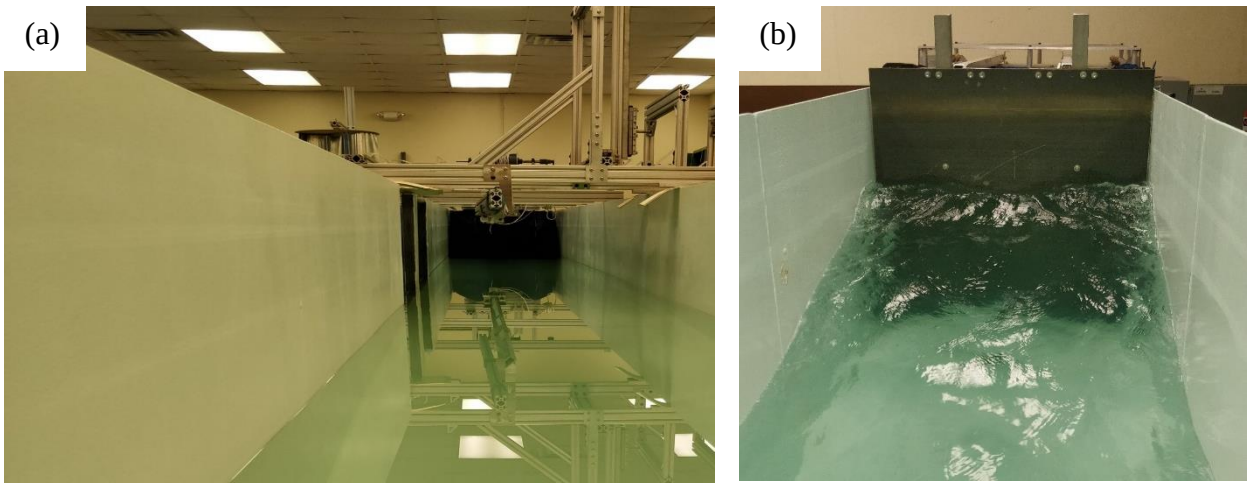

Fig. 11. (a) Wave tank facility; (b) single flap type wave maker.

lessen the impact of the reflection wave on the WEC. The wave generator has a single flap. Figure 11 illustrates the system, which consists of a paddle rotating between two places at a predetermined frequency to produce a regular wave that travels from the right side to the left. A variable speed motor is used to propel the wave paddle ahead at the water's surface. The frequency ratio between

the motor and the wave paddle is 50:1. The crank radius may be changed to vary the wave height. There are two observation windows made of heavy plate glass to facilitate experiments.

Experimental observations for fixed power take-off

The performed experimental testing is classified as (i) analysis of the converter behavior and (ii) converter performance assessment. Converter behavior is analyzed using the 1:5 scaled model, while the 1:3 scaled model is used for performance assessment.

Analysis of the converter behavior in the vertical orientation

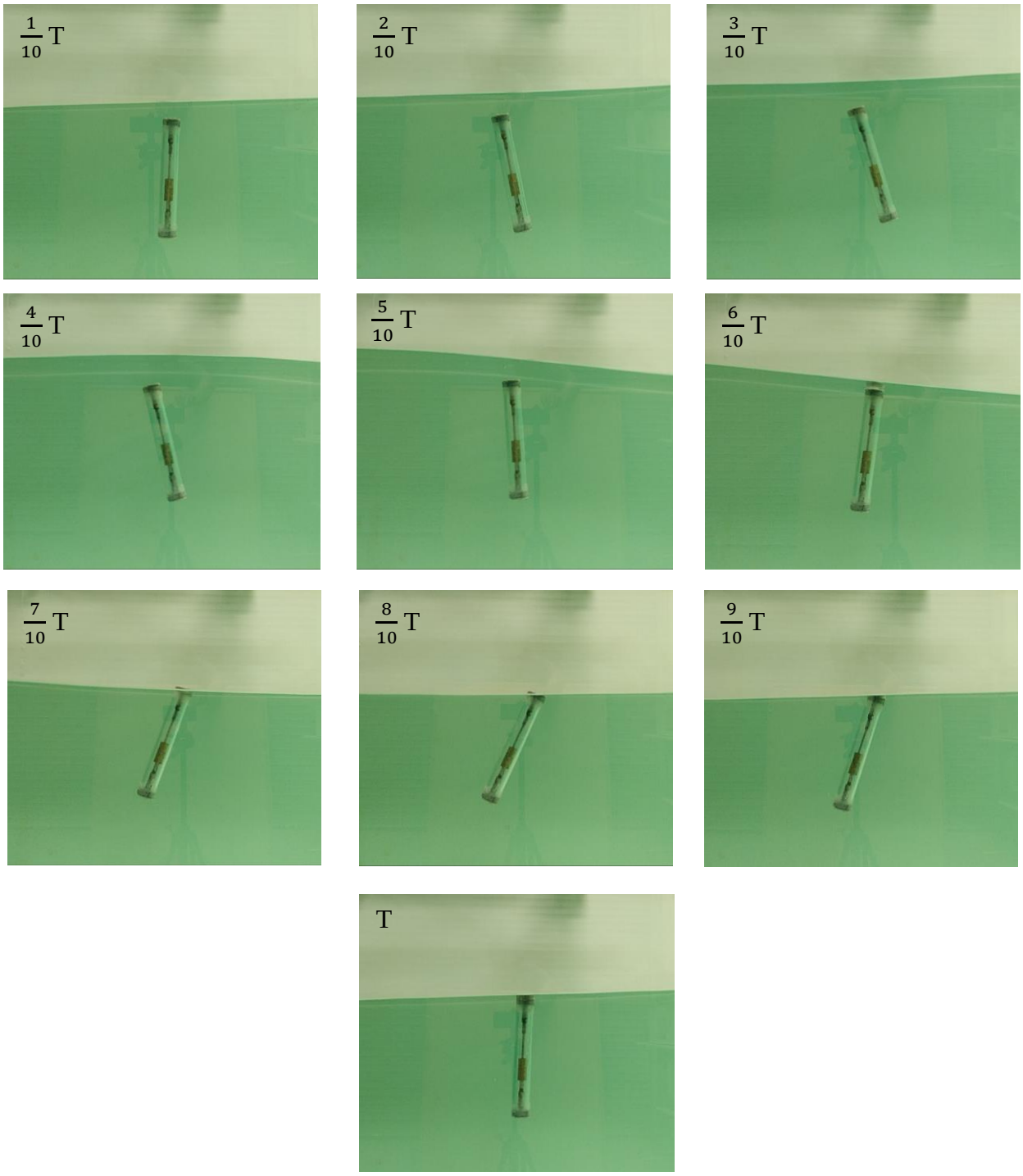

Fig. 12. PTO fixed AUV motion in wave frequency 0.5 Hz and height 0.113 m. Here, T means the wave period.

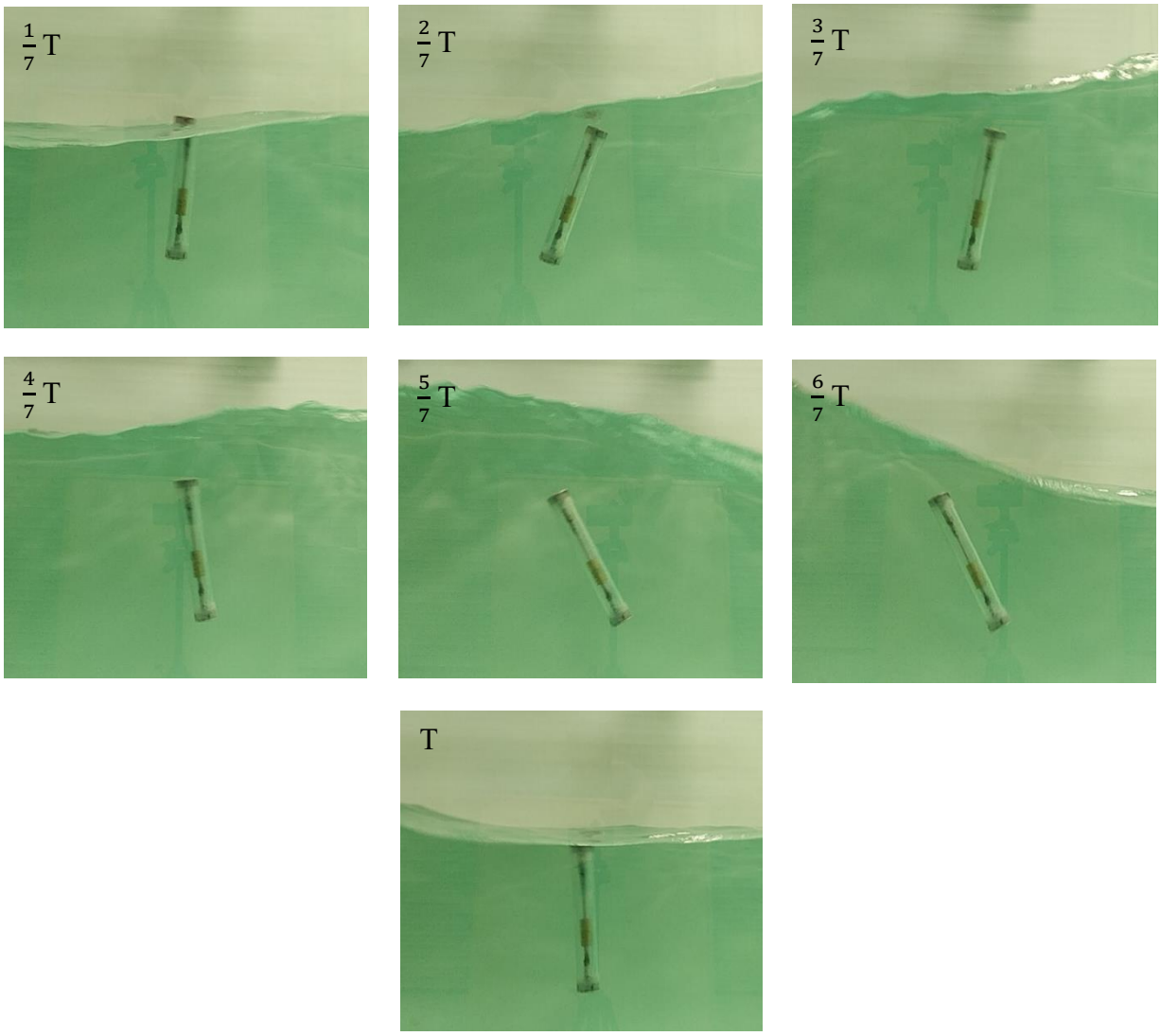

Fig. 13. PTO fixed AUV motion in wave frequency 0.7 Hz and height 0.242 m. Here, T means the wave period.

Analysis of the converter behavior in the horizontal orientation

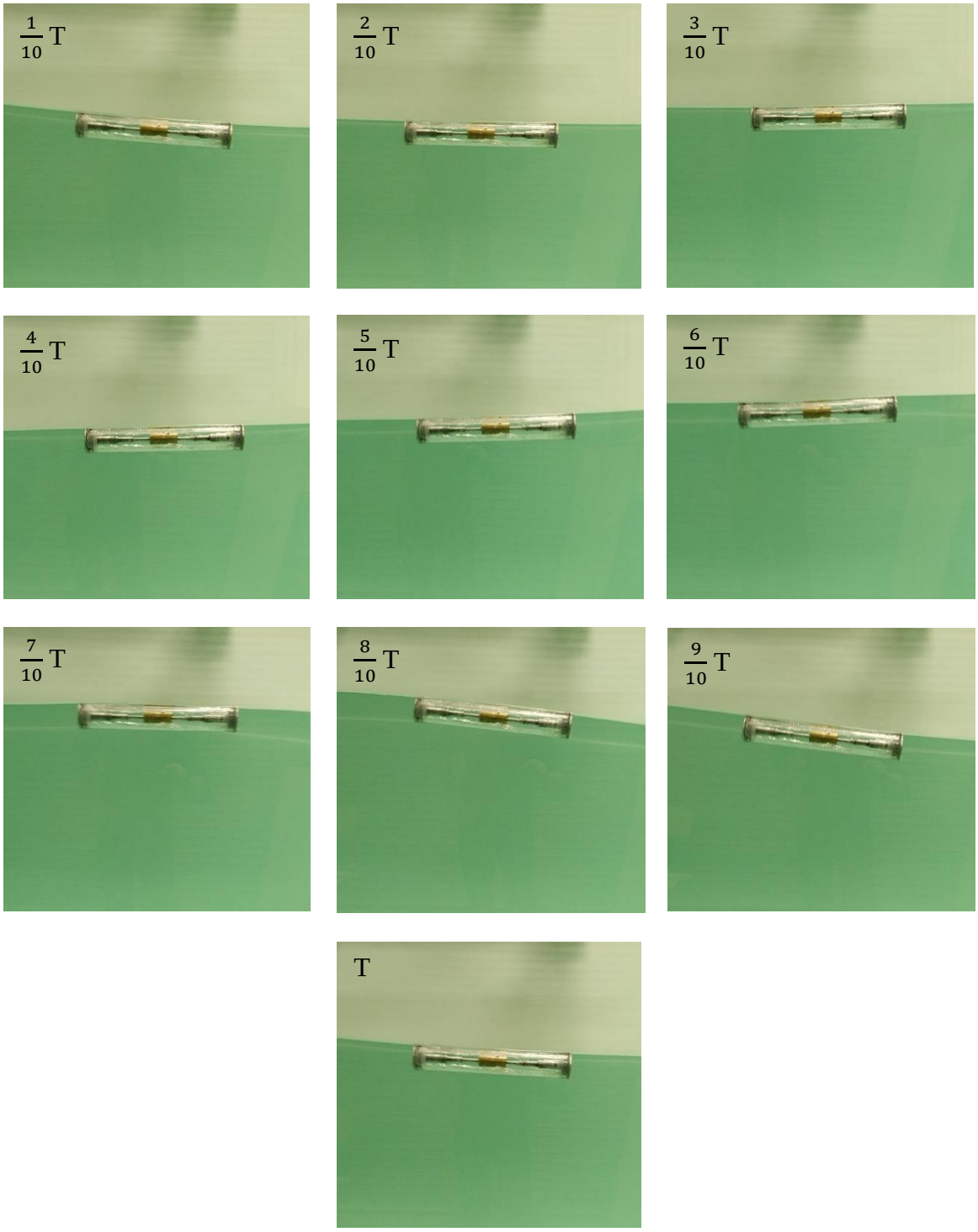

Fig. 14. PTO fixed AUV motion in wave frequency 0.5 Hz and height 0.113 m. Here, T means the wave period.

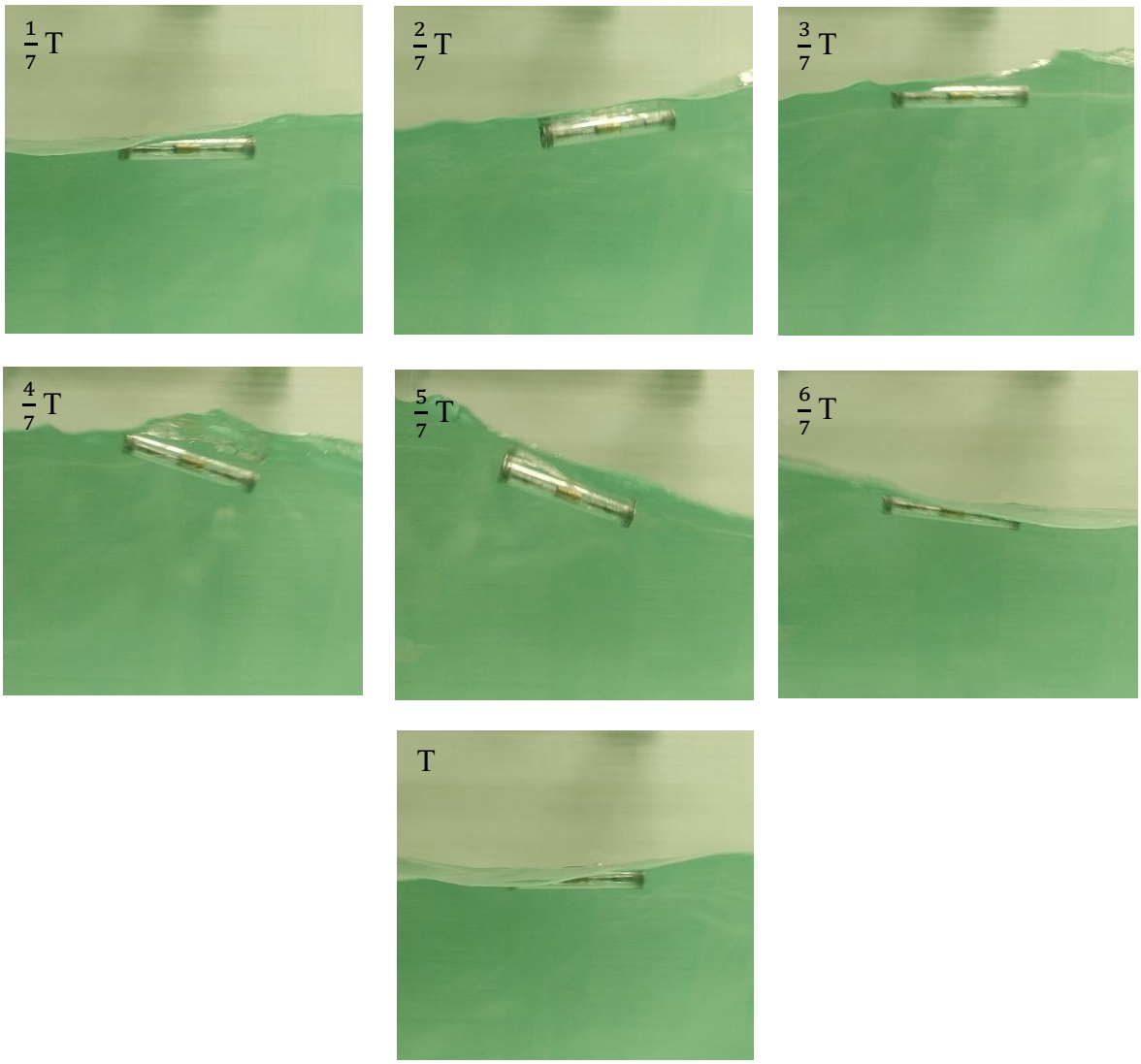

Fig. 15. PTO fixed AUV motion in wave frequency 0.7 Hz and height 0.242 m. Here, T means the wave period.

Numerical Modeling

Numerical modeling is a critical step to iteratively improve a WEC's performance for cost effectiveness and reliability. A general energy conversion cycle of a hull encapsulated WEC consists of three typical processes. As the WEC's hull moves in waves, the wave energy is partially absorbed by the hull through wave-WEC interaction. Then an onboard PTO unit converts the hull absorbed energy into a form that can directly drive an appropriate electric generator. Sequentially, the electric generator produces electricity (Sheng, 2019). In this thesis we are going to focus on the onboard PTO unit only.

Numerical Modeling Strategy

The numerical modeling section aims to simulate the motion of the mass affected by the spring and damper system inside the encapsulated hull, as shown in Figure 6 and 7, for both vertical and horizontal orientation. The motion with the time of the oscillating mass for different spring constants and damping coefficients can be solved using the equations 1-3 for vertical orientation and 4-6 for horizontal orientation. The wave parameters: frequency, and wave height for different real life sea conditions can be used as an input to the simulation. The average power $\bar{P}$ from the PTO from both orientations can be evaluated using Equation 7.

The position and velocity of the oscillating mass are solved using the second-order differential equations. MATLAB ode45 function is used to solve the differential equations. Ode solvers do not work with higher-order differential equations. So, a system of first order differential equations has been used for that. The simulation parameters for the 1:5 scaled model have been tabulated in Table 1.

Part of the difficulty in solving some systems of ODEs is determining an appropriate time to stop the calculation. In our case, the oscillating mass hits the end stops twice—at $X_{PTO} > z_0$ and $X_{PTO} < -z_0$. When $|X_{PTO}| \leq z_0$ or the oscillating mass is in between the two extreme positions, the spring force acting on it is only due to the compression spring. But at the two stroke ends the disk spring of stiffness $k = \frac{nmg}{z_0}$ gets engaged. So, we need to determine the exact time of this events to occur to stop the calculation of previous equation and start solving the new equation of the corresponding interval. We have used MATLAB event function to detect when certain events occur during the solution of our ODE.

Table 1: Simulation Parameters for the 1:5 Scaled Model.

Simulation Parameters	1:5 Scaled Model
Oscillating mass, m (kg)	0.345
Half of total sliding length, z_0 (m)	0.034
Wave frequency, f_W (Hz)	0.3, 0.5, 0.6, 0.7
Wave height, H (m)	0.137, 0.113, 0.198, 0.242
Spring constant, k_{PTO} (N/m)	0-60 (vertical orientation) 0-120 (horizontal orientation)
Damping coefficient, C_{PTO} (Ns/m)	0-20 (vertical orientation) 0-60 (horizontal orientation)
Disk spring constant, n	100
Angular oscillation amplitude, θ_0	$\frac{\pi}{3}°$
Initial phase angle, ϕ_0	0°
Static equilibrium constant, ε	-1
Initial condition, i_C	$z_{PTO} = 0, \frac{dz_{PTO}}{dt} = 0$

Numerical Simulation Result

Numerical simulation has been done for both vertical and horizontal orientation of the AUV. The power curves and position-velocity-time plots are demonstrated in Figure 16-19.

Vertical orientation.

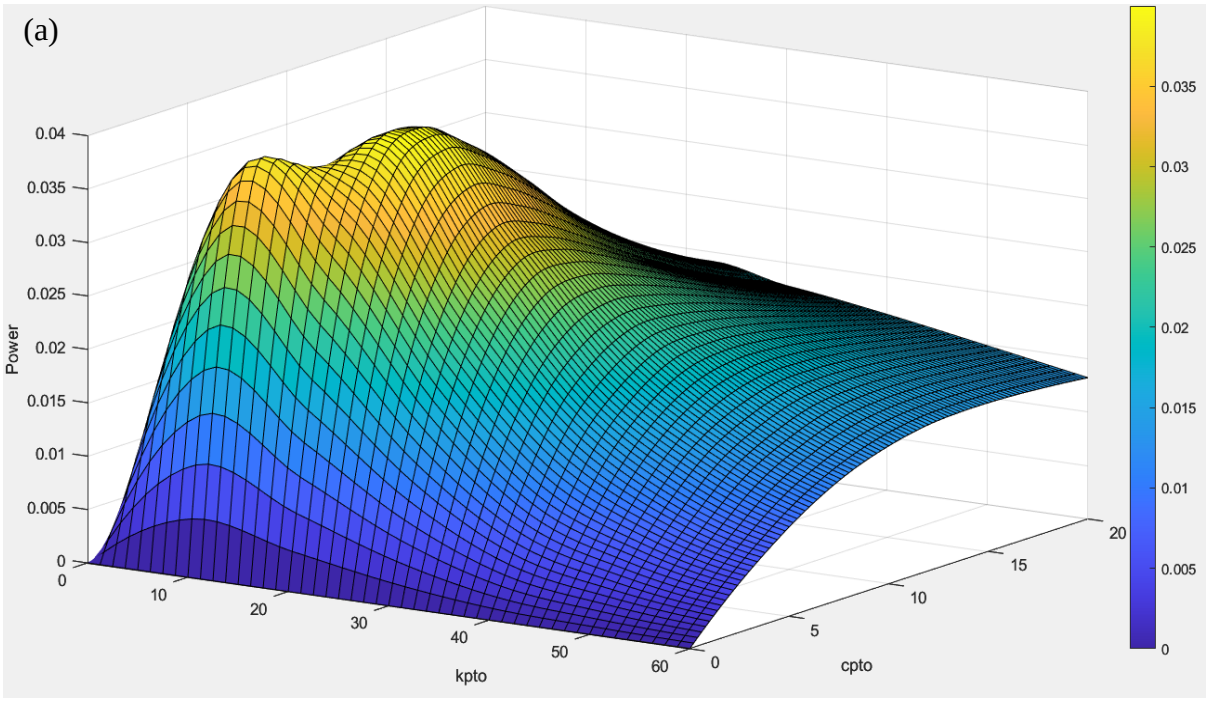

Maximum power 0.04 W for $k_{PTO} = 21.25 \frac{N}{m}$ *and* $C_{PTO} = 5.6\ Ns/m$.

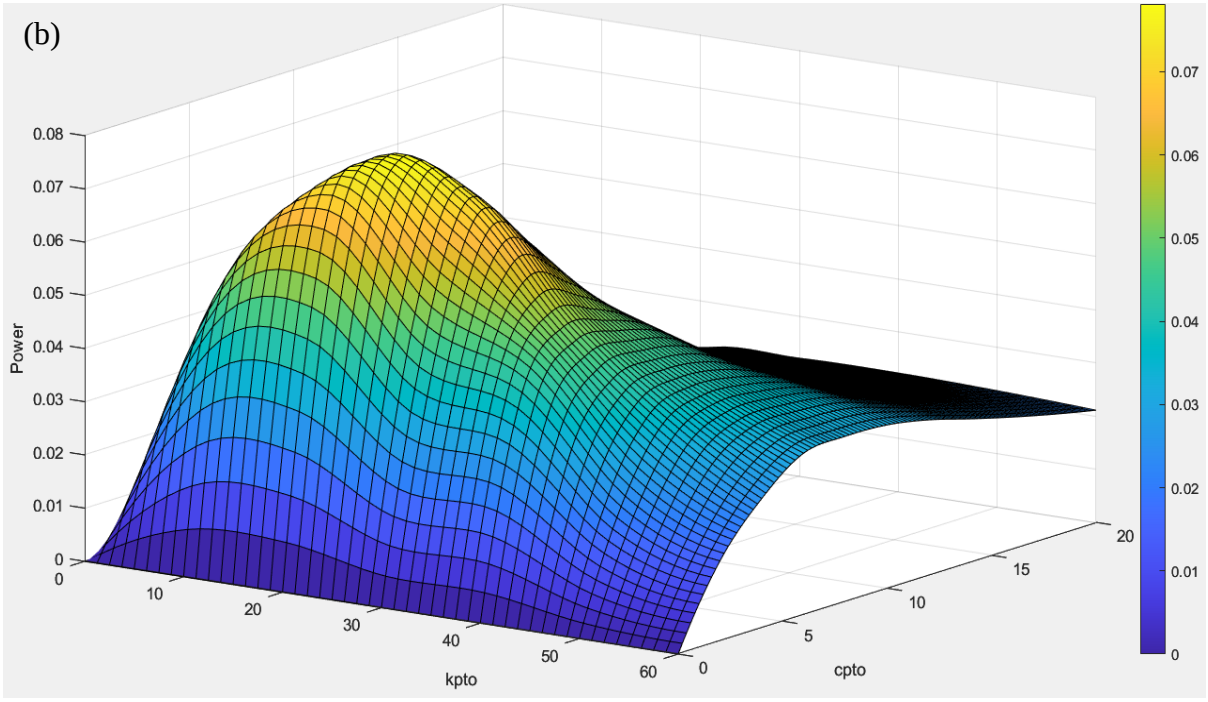

Maximum power 0.0781 W for $k_{PTO} = 23.75 \frac{N}{m}$ *and* $C_{PTO} = 4.2\ Ns/m$.

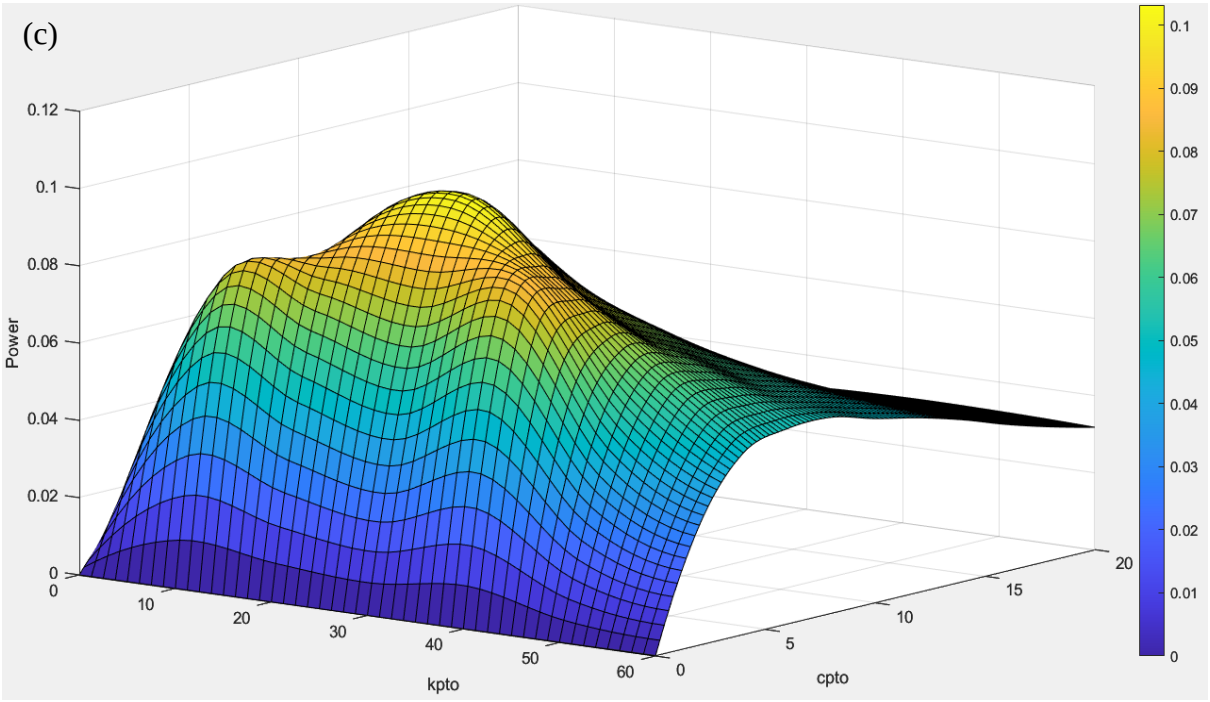

Maximum power 0.1032 W for $k_{PTO} = 28.75\ N/m\ and\ C_{PTO} = 4.4$ Ns/m.

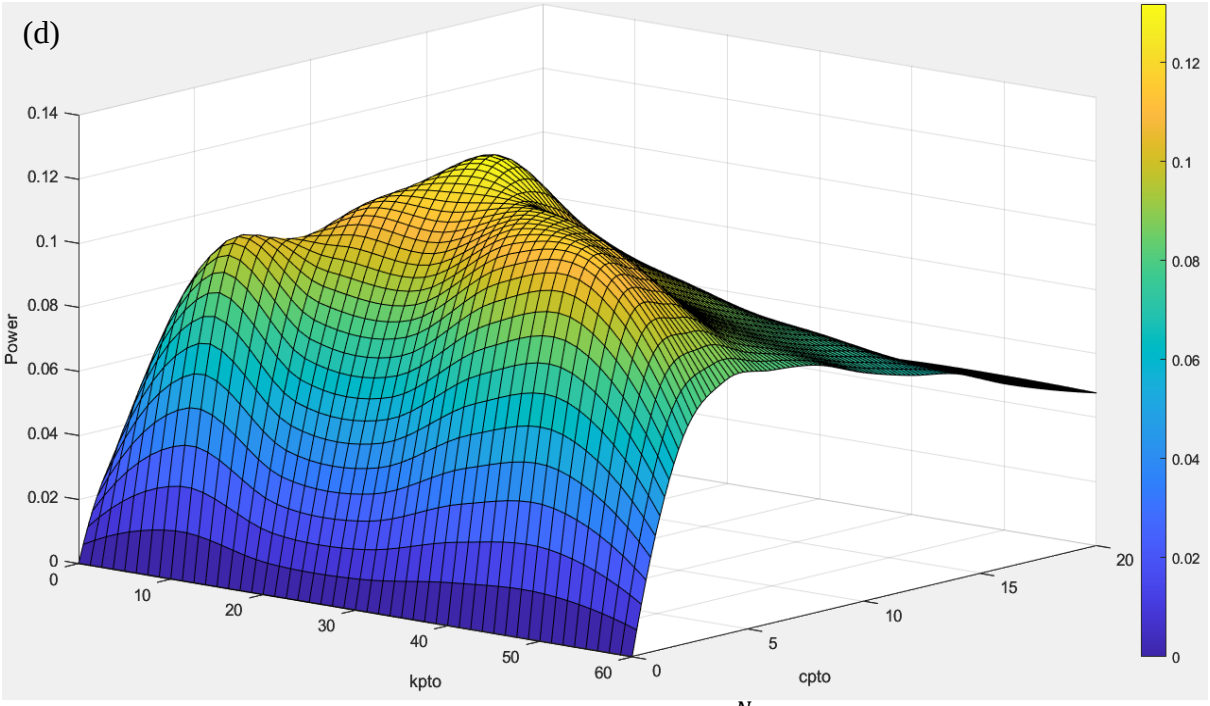

Maximum power 0.1318 W for $k_{PTO} = 30\frac{N}{m}\ and\ C_{PTO} = 6\ Ns/m$.

Fig. 16. Power curves; (a) wave of frequency 0.3 Hz and height 0.137 m, (b) wave of frequency 0.5 Hz and height 0.113 m, (c) wave of frequency 0.6 Hz and height 0.198 m, and (d) wave of frequency 0.7 Hz and height 0.242 m.

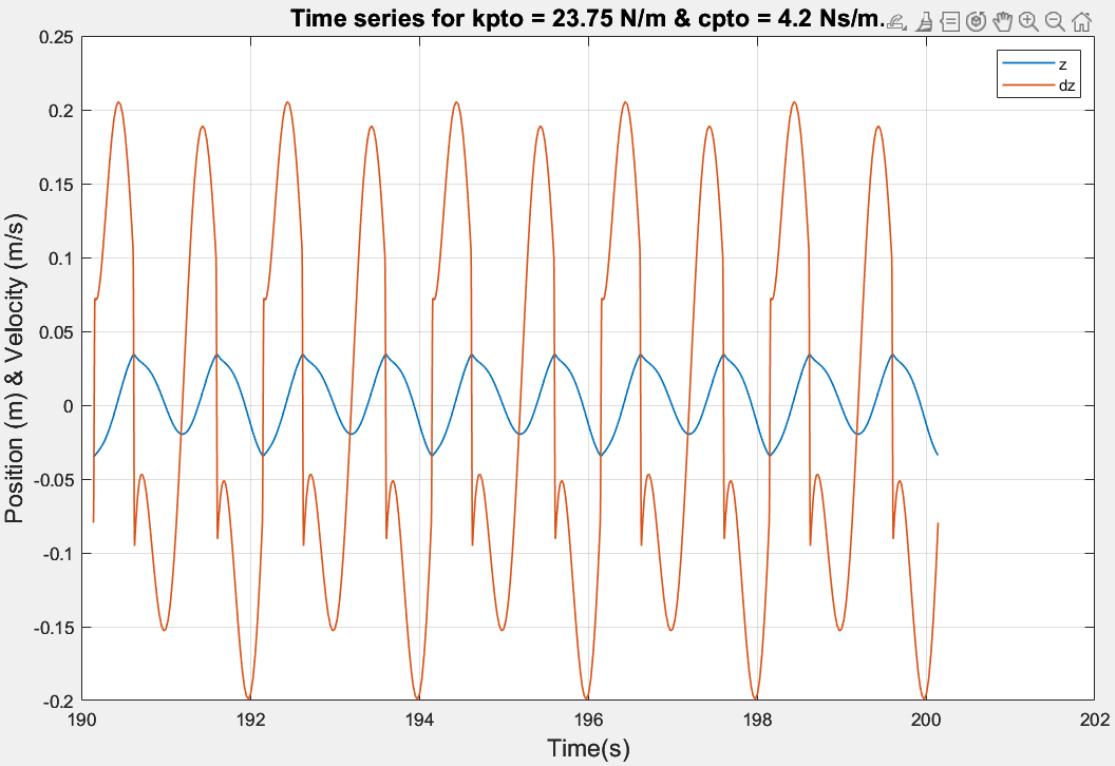

Average power: 0.0755 W

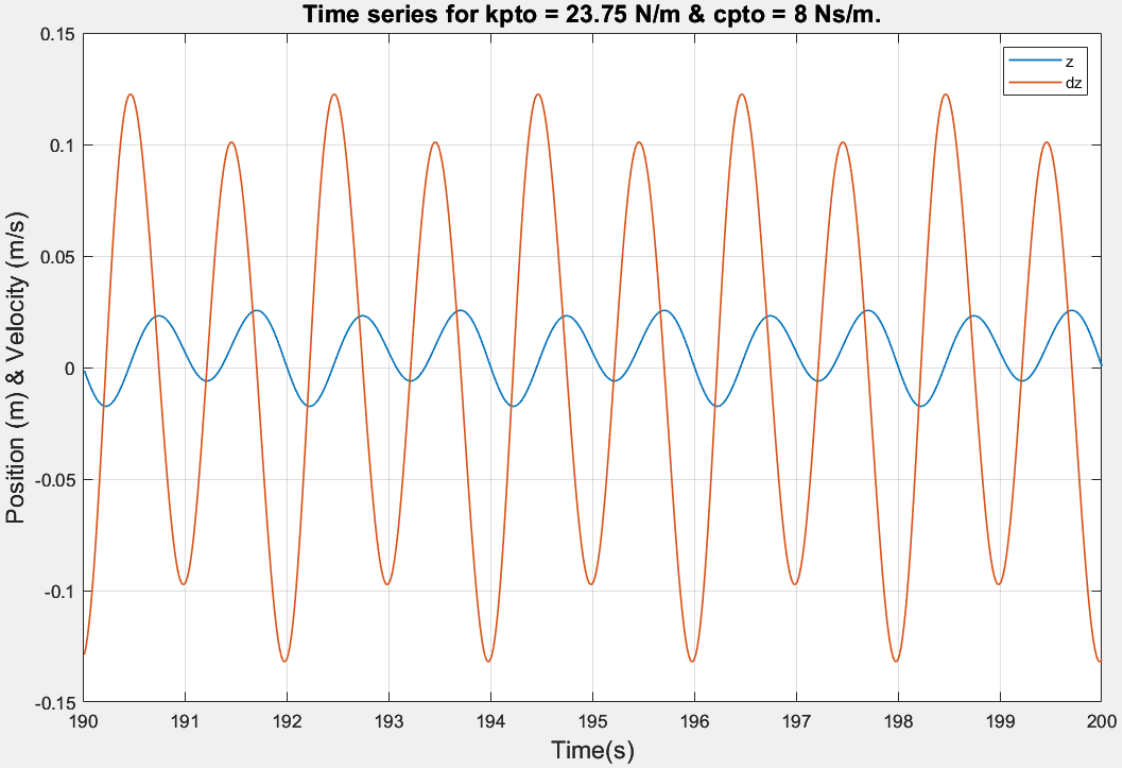

Average power: 0.0523W

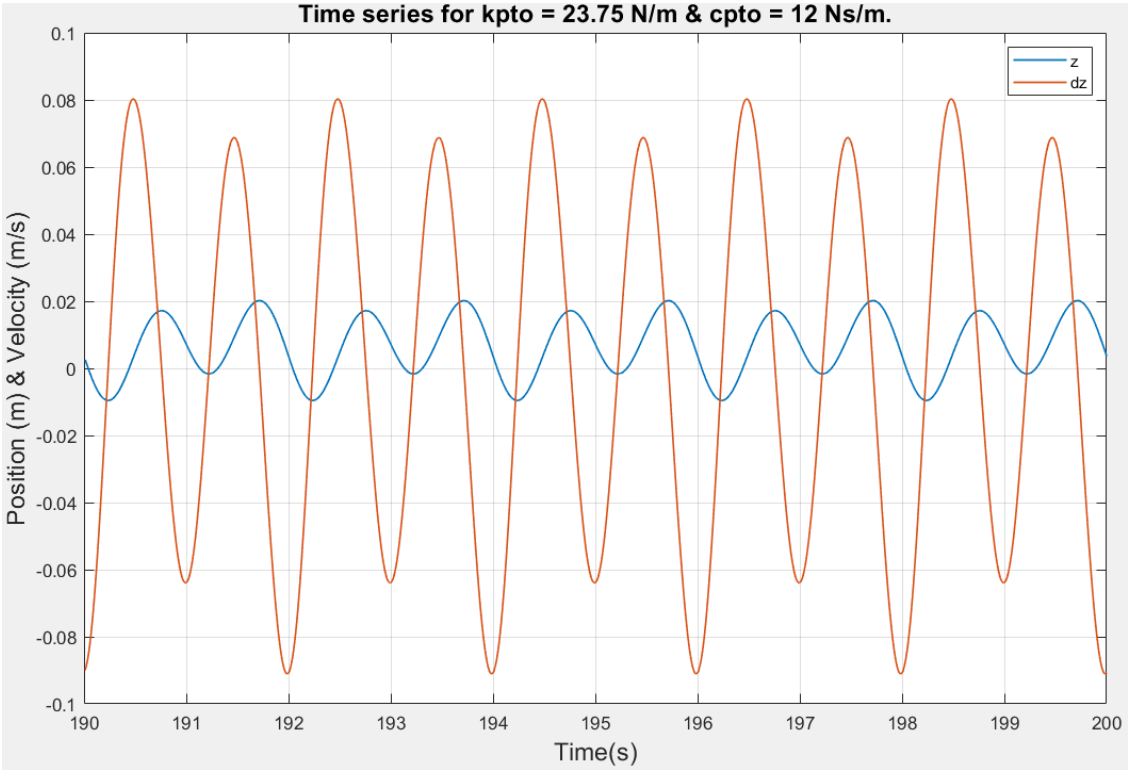

Average power: 0.0355W

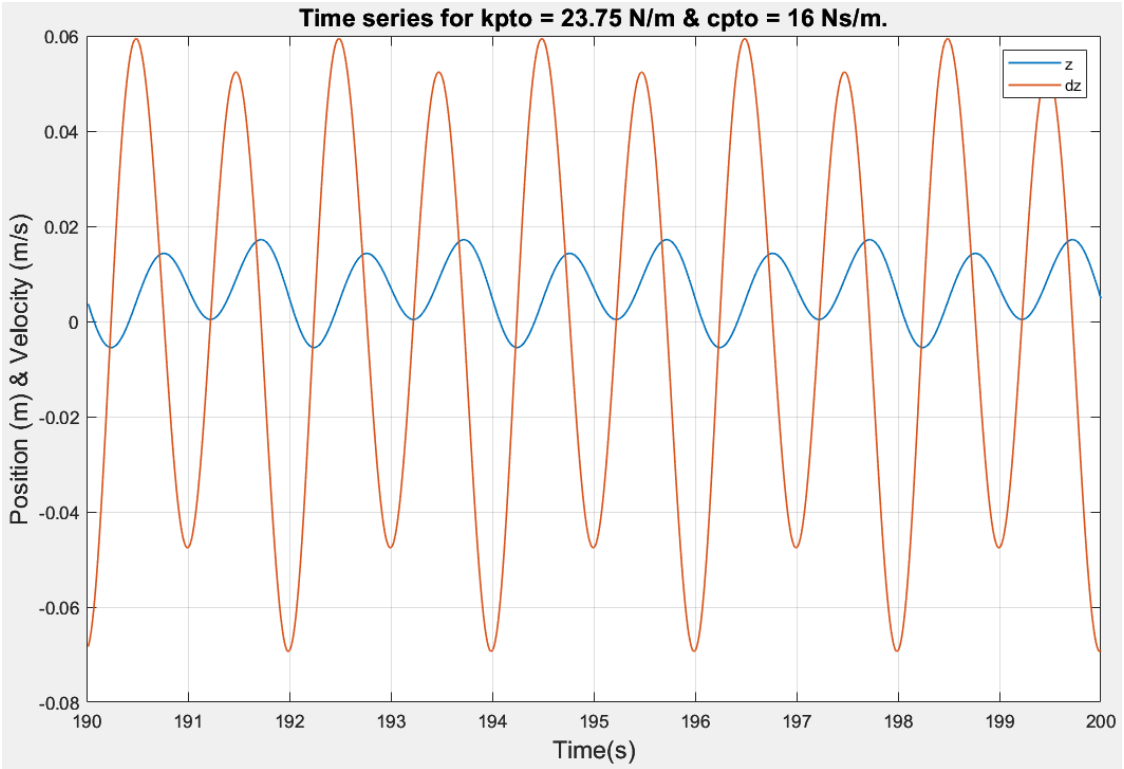

Average power: 0.0268 W

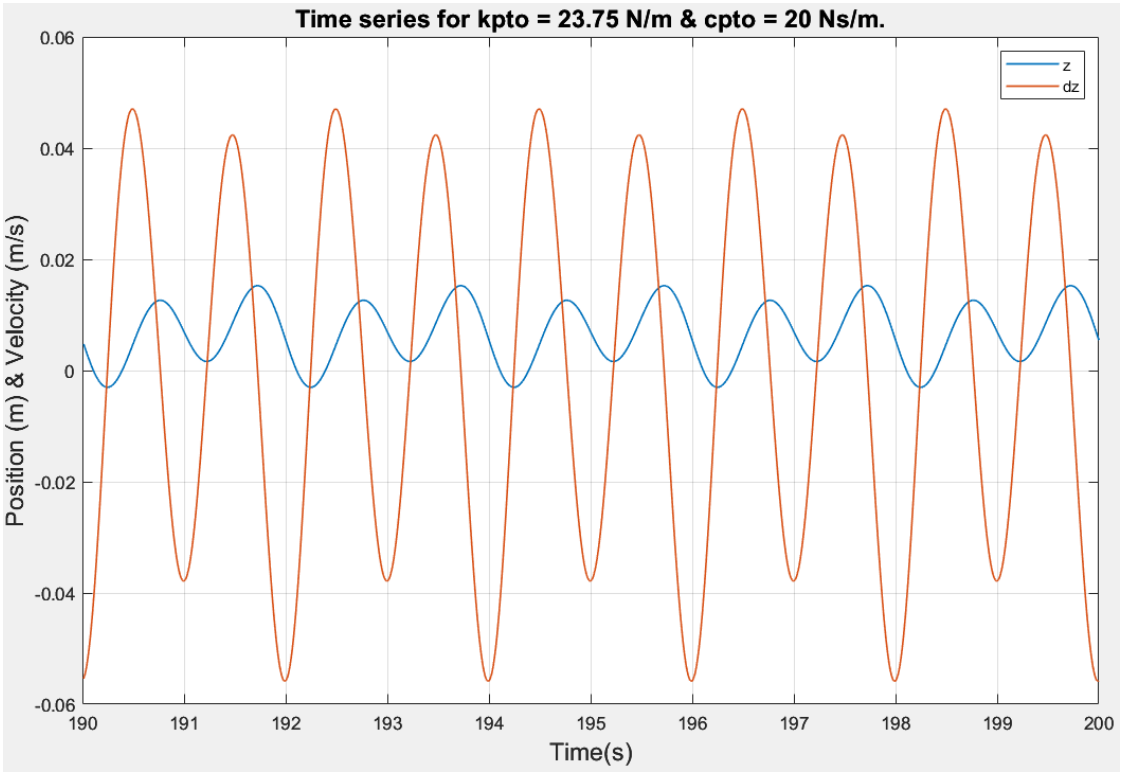

Average power: 0.0215 W

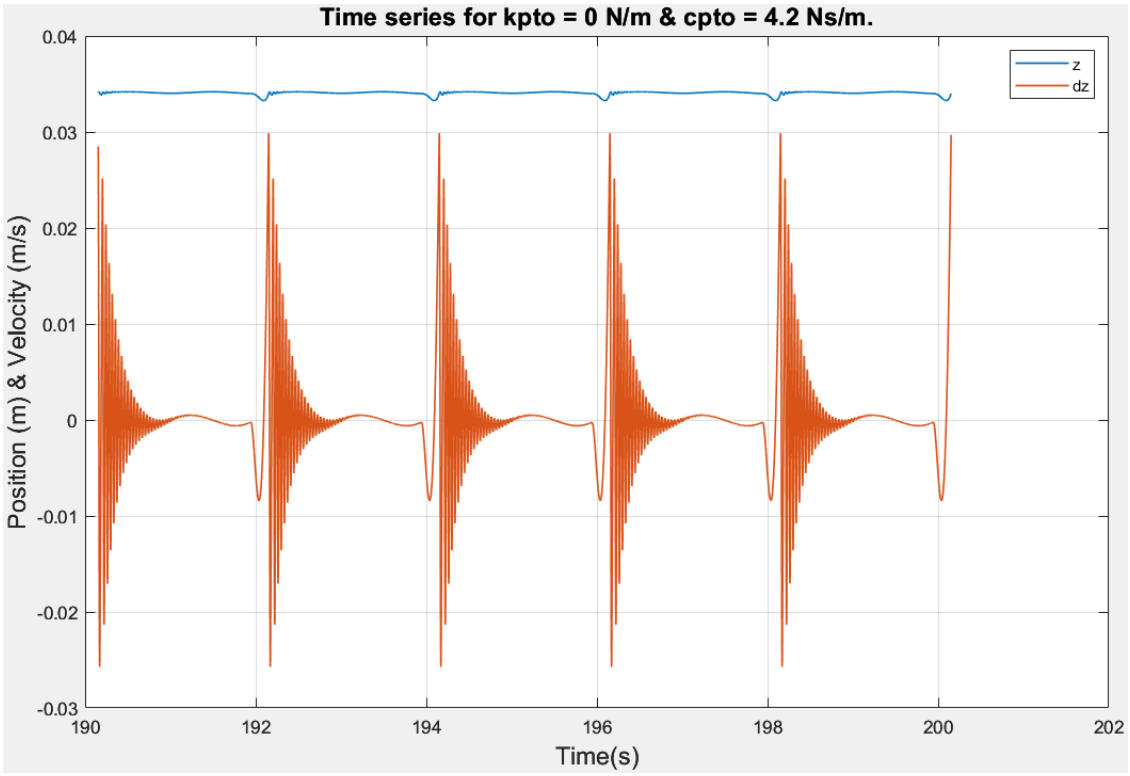

Average power: 0.0001 W

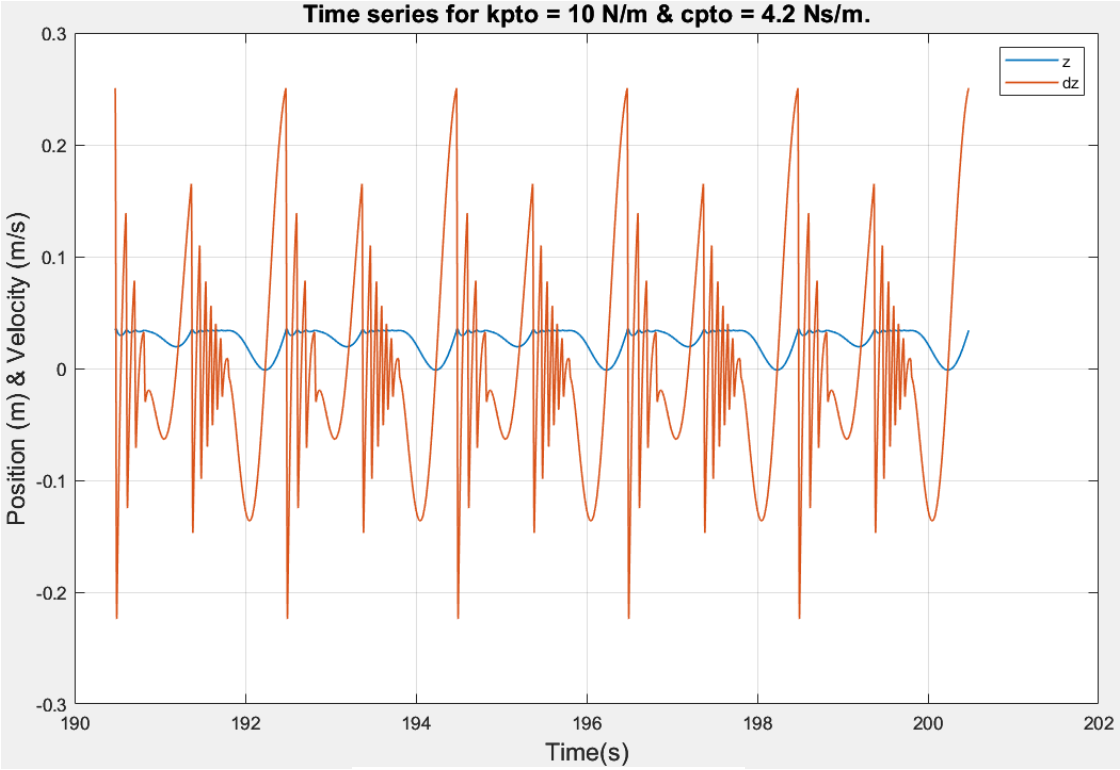

Average power: 0.0339 W

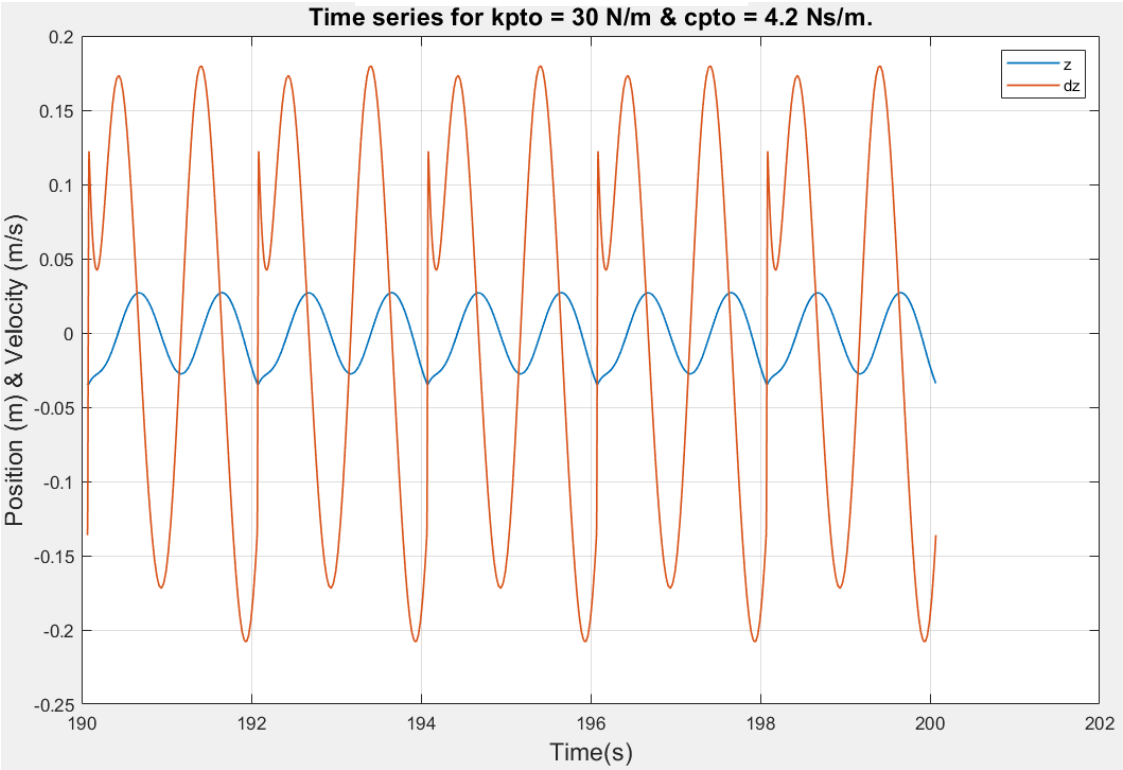

Average power: 0.0705 W

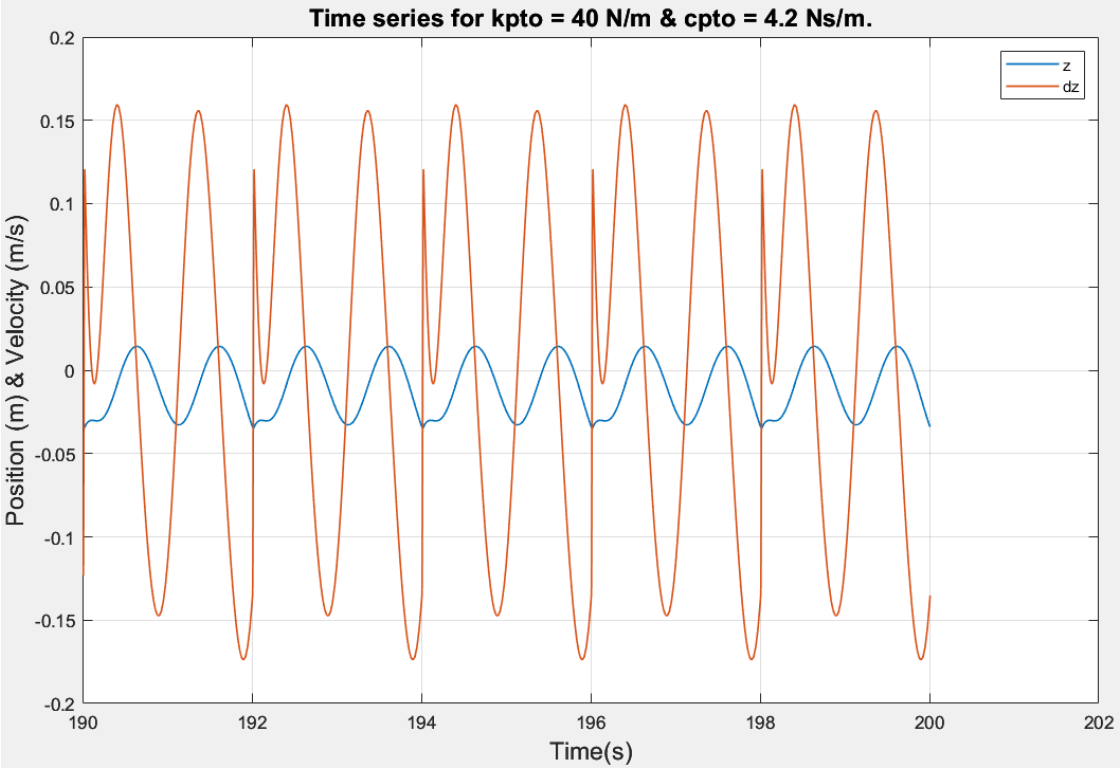

Average power: 0.0509 W

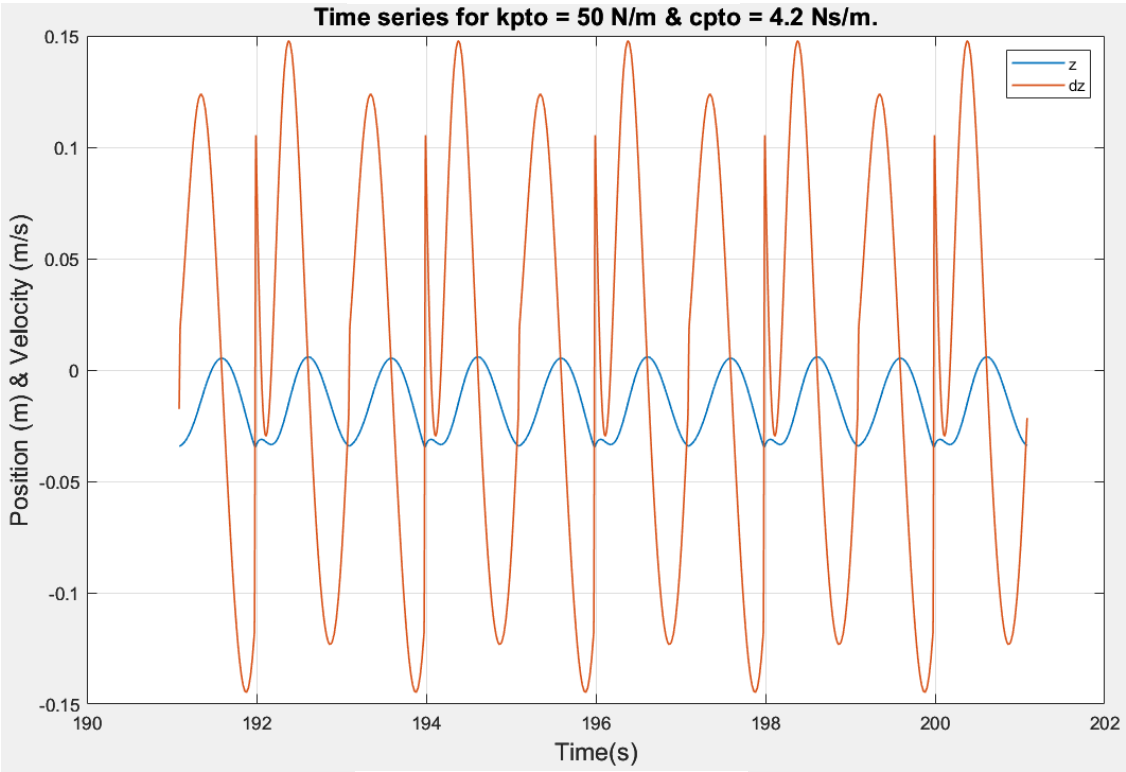

Average power: 0.0363 W

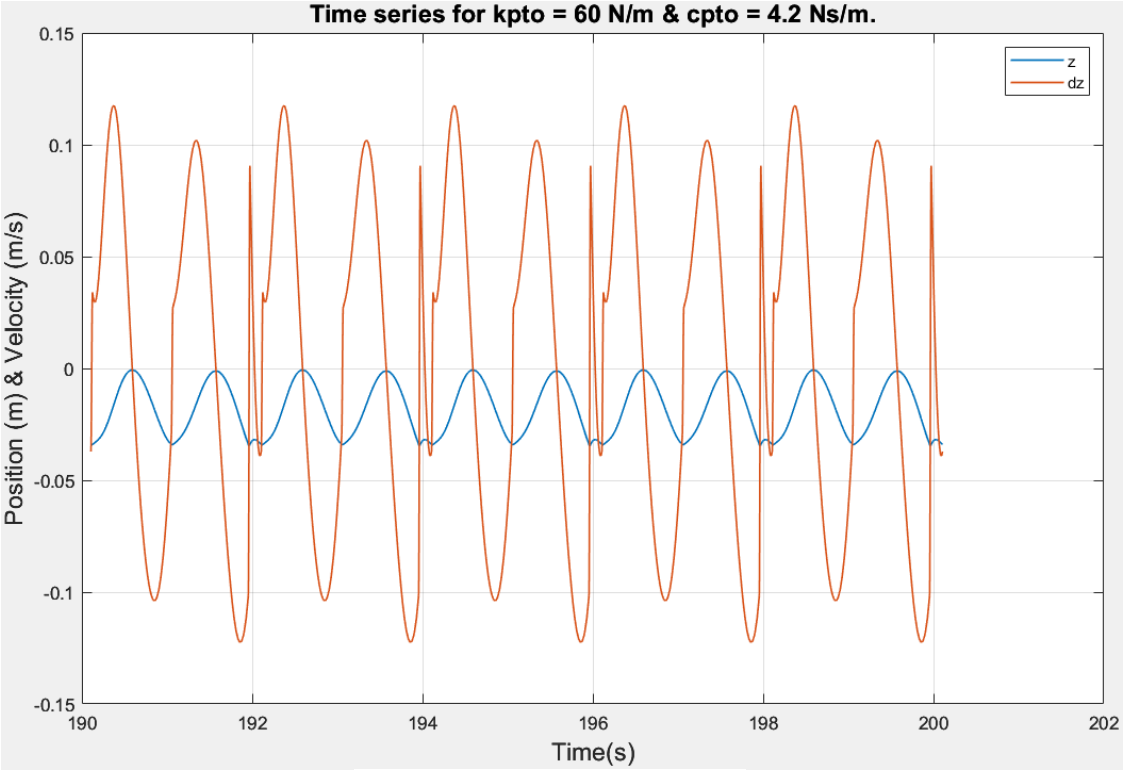

Average power: 0.0251 W

Fig. 17. Position-velocity-time plots for a wave of frequency 0.5 Hz and height 0.113 m.

Horizontal orientation.

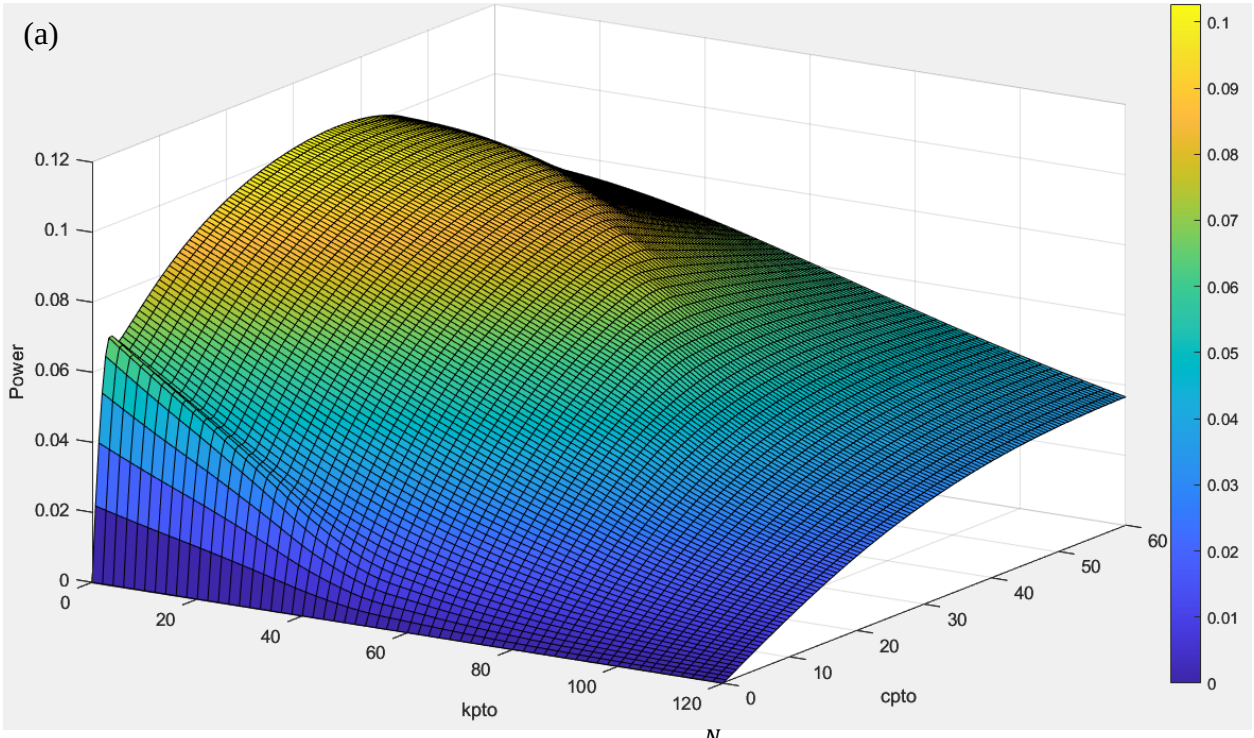

Maximum power 0.1027 W for $k_{PTO} = 0\frac{N}{m}$ and $C_{PTO} = 36.5\ Ns/m$.

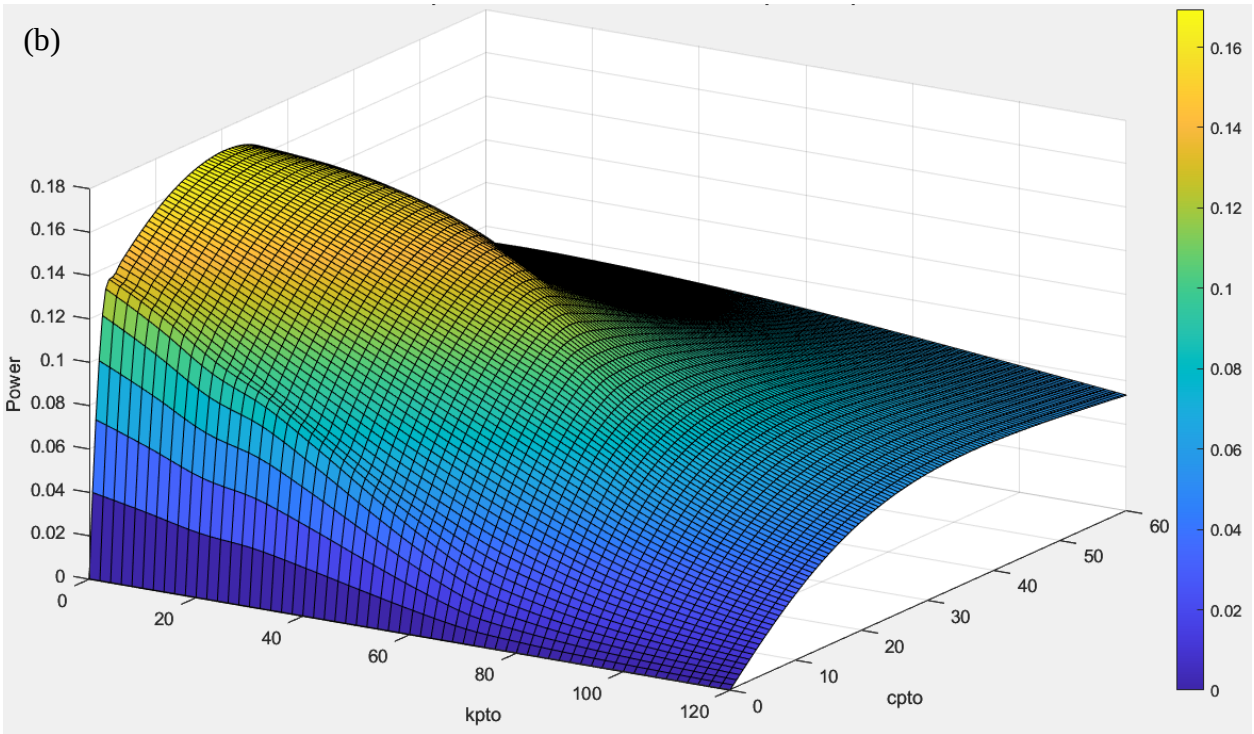

Maximum power 0.1694 W for $k_{PTO} = 0\frac{N}{m}$ and $C_{PTO} = 20.5\ Ns/m$.

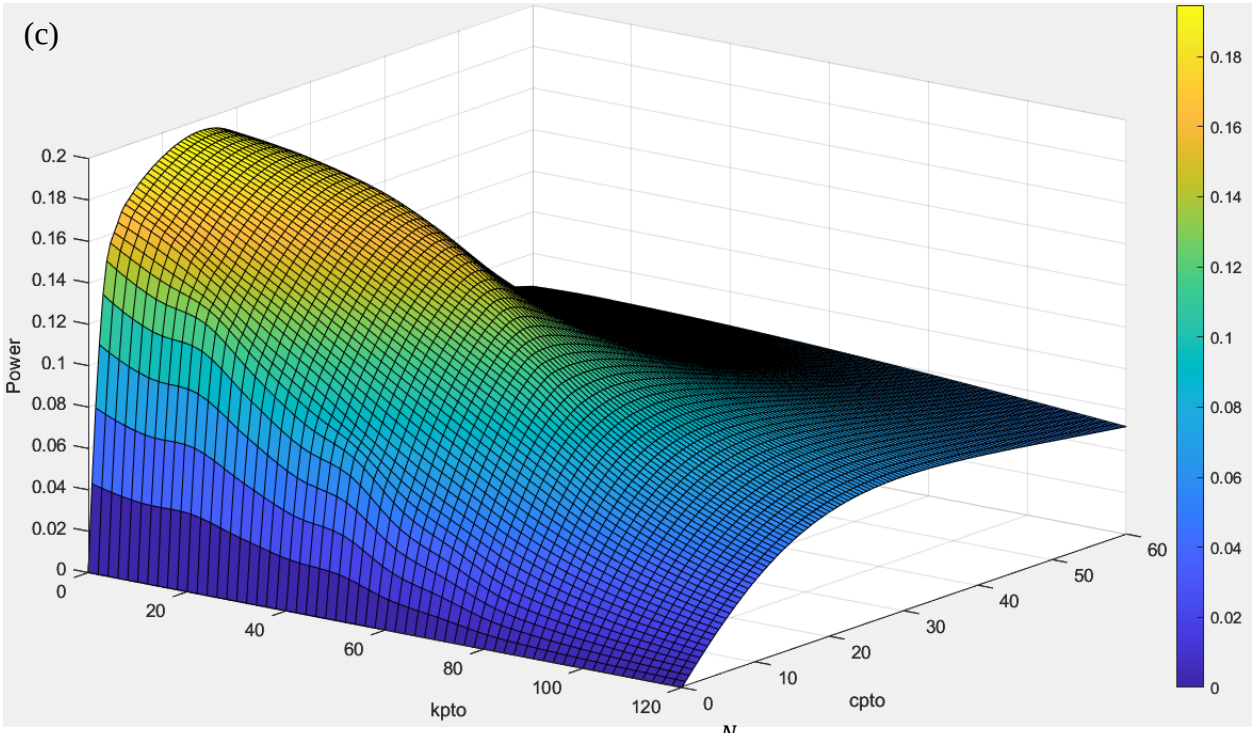

Maximum power 0.1947 W for $k_{PTO} = 0 \frac{N}{m} and\ C_{PTO} = 15.5\ Ns/m.$

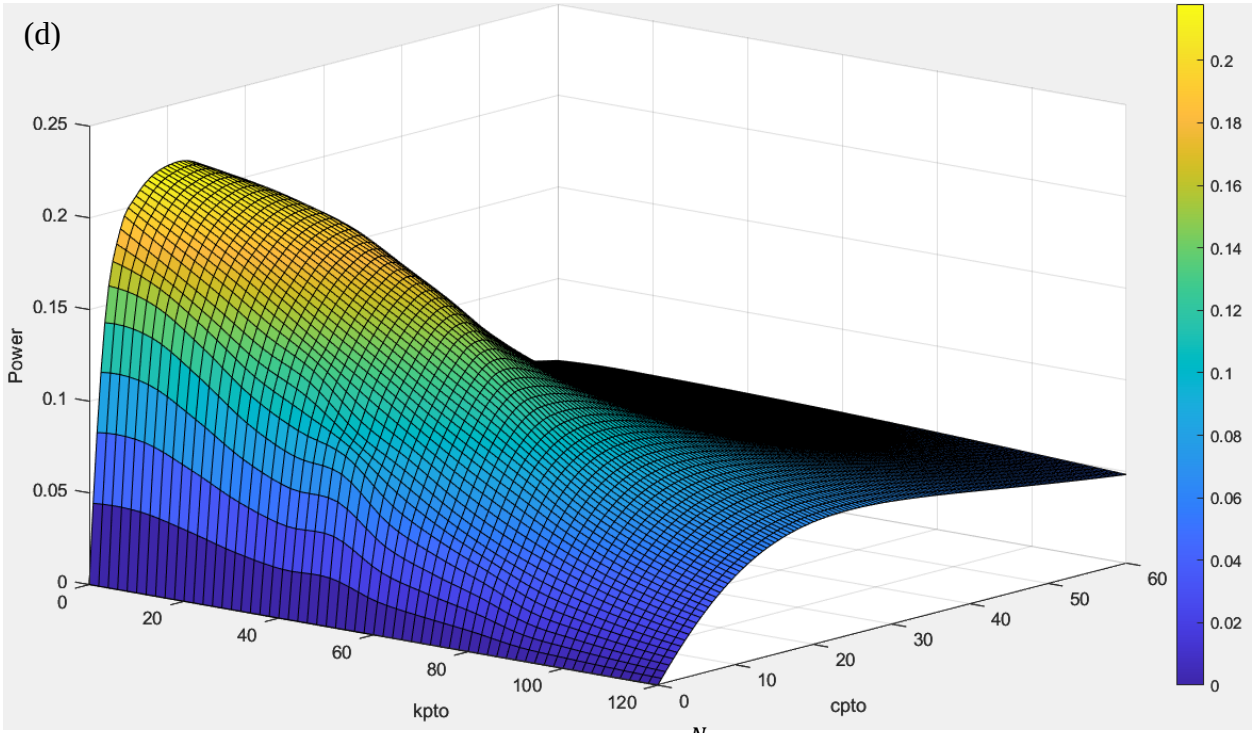

Maximum power 0.2180 W for $k_{PTO} = 0 \frac{N}{m} and\ C_{PTO} = 11.5\ Ns/m.$

Fig. 18. Power curves; (a) wave of frequency 0.3 Hz and height 0.137 m, (b) wave of frequency 0.5 Hz and height 0.113 m, (c) wave of frequency 0.6 Hz and height 0.198 m, and (d) wave of frequency 0.7 Hz and height 0.242 m.

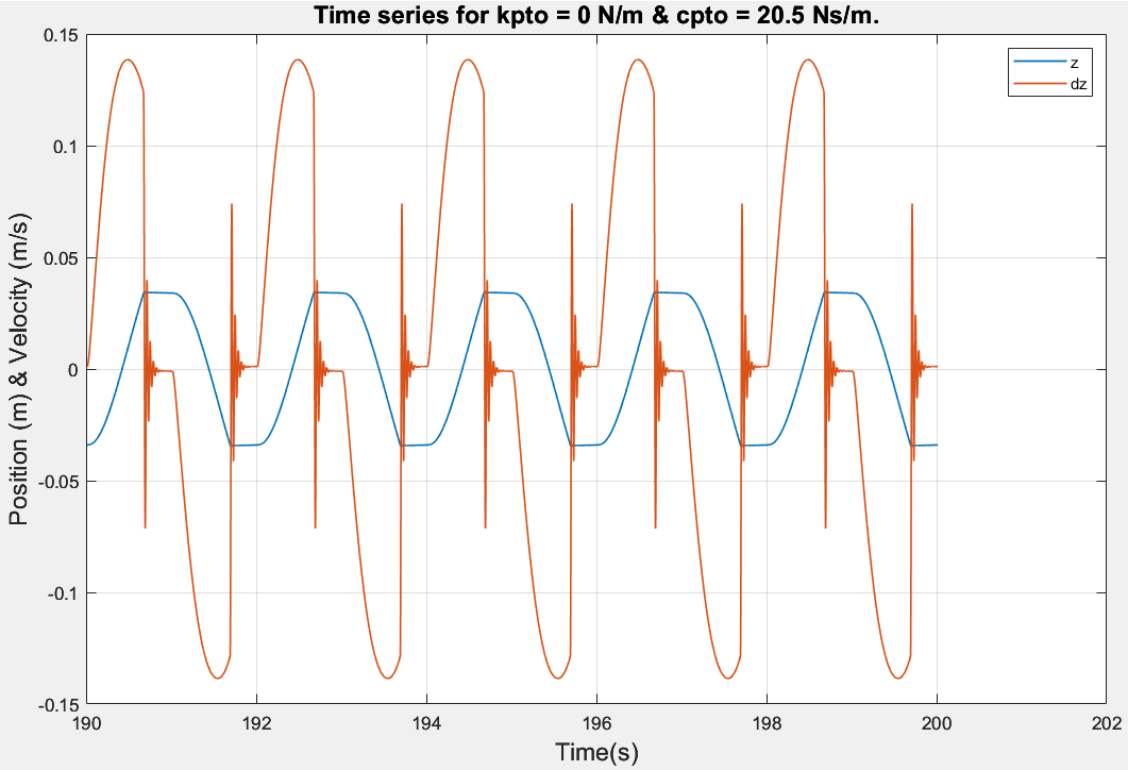

Average power: 0.1694 W

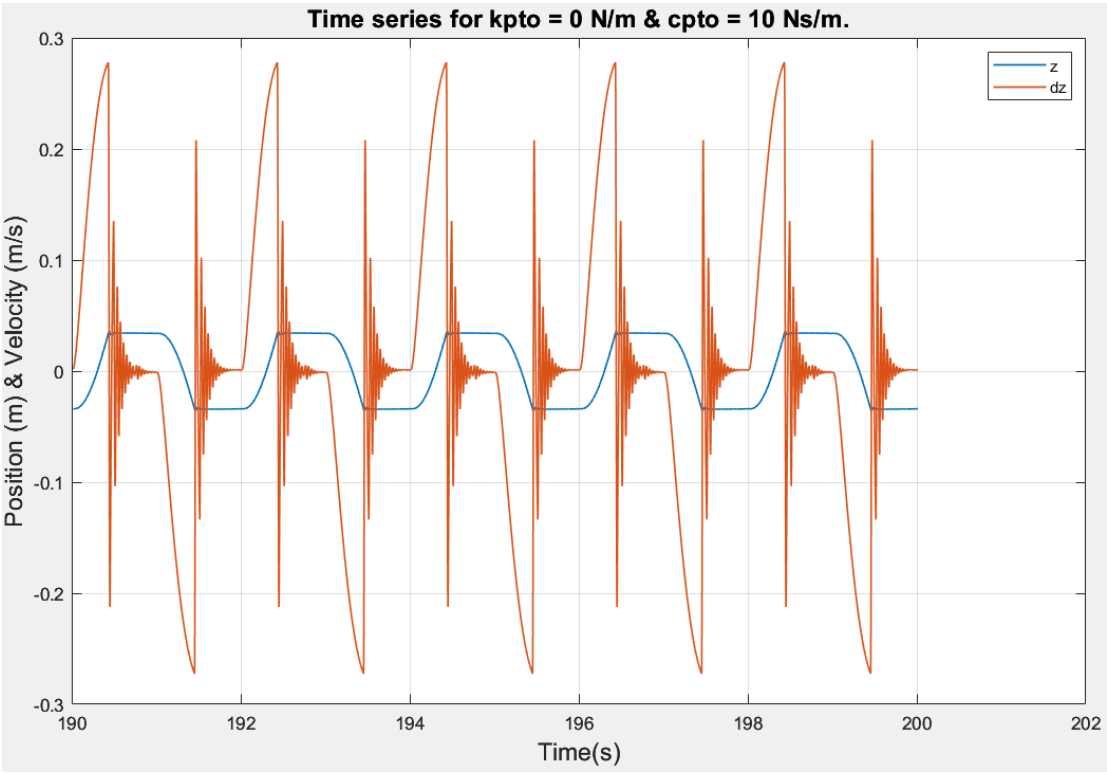

Average power: 0.1556 W

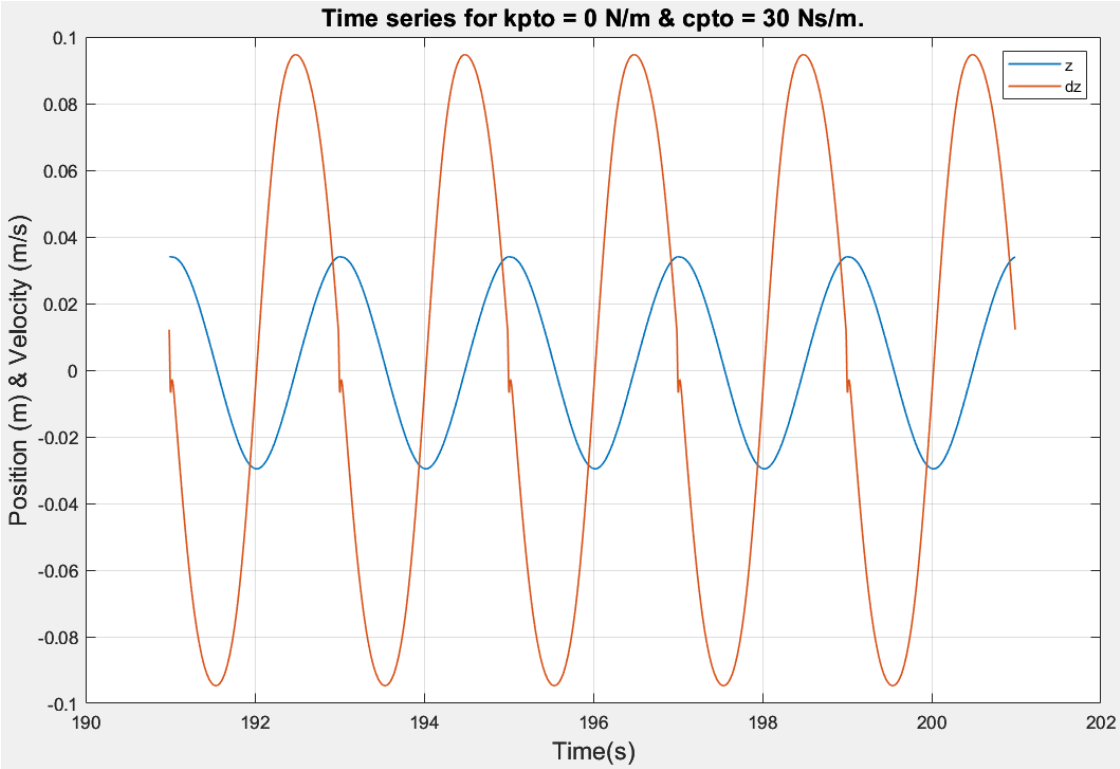

Average power: 0.1463 W

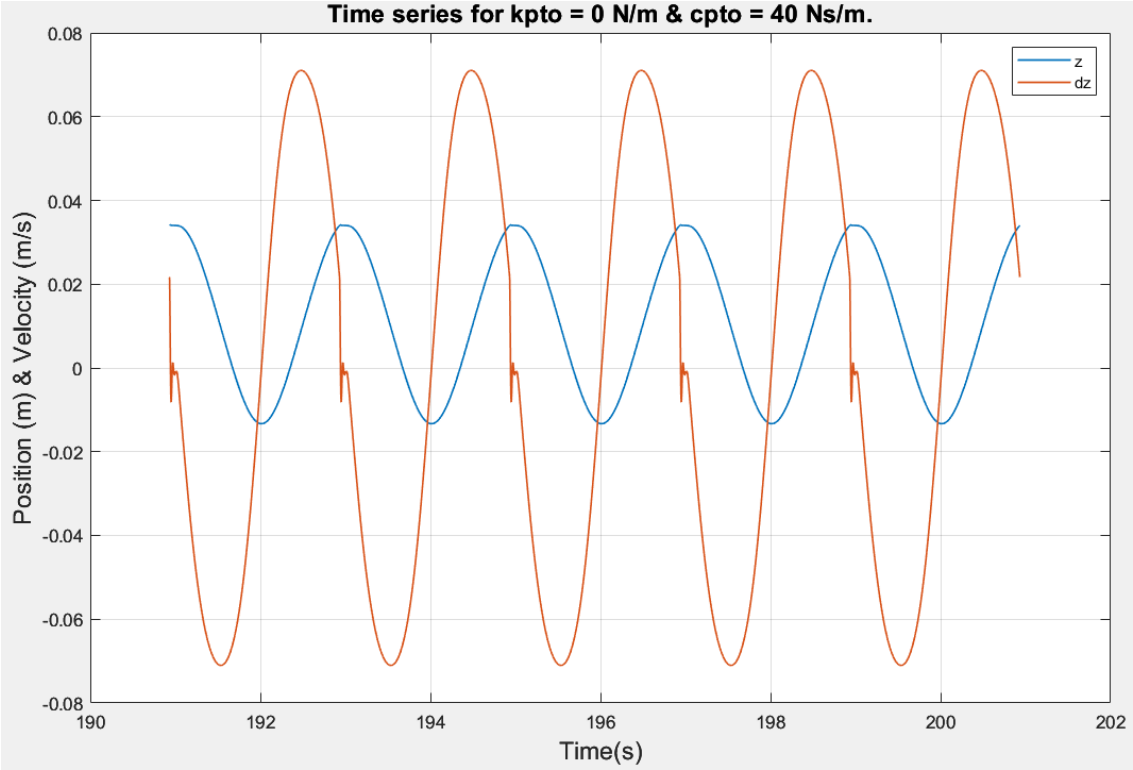

Average power: 0.1096 W

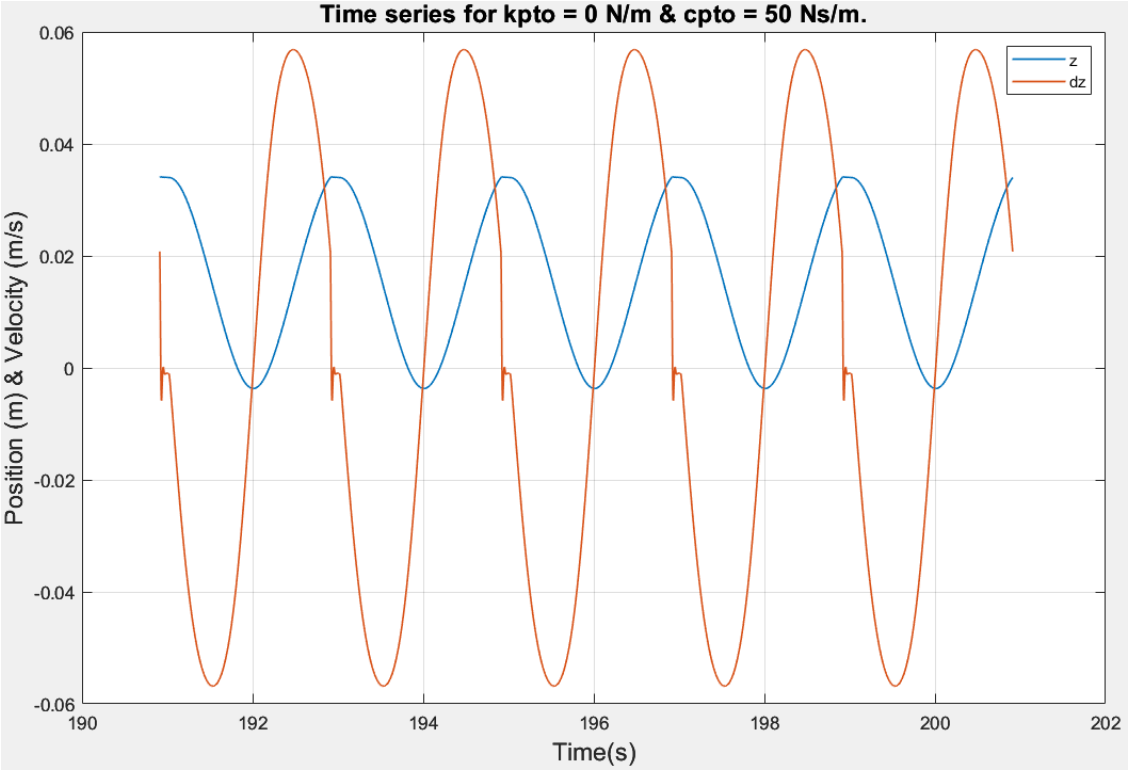

Average power: 0.0876 W

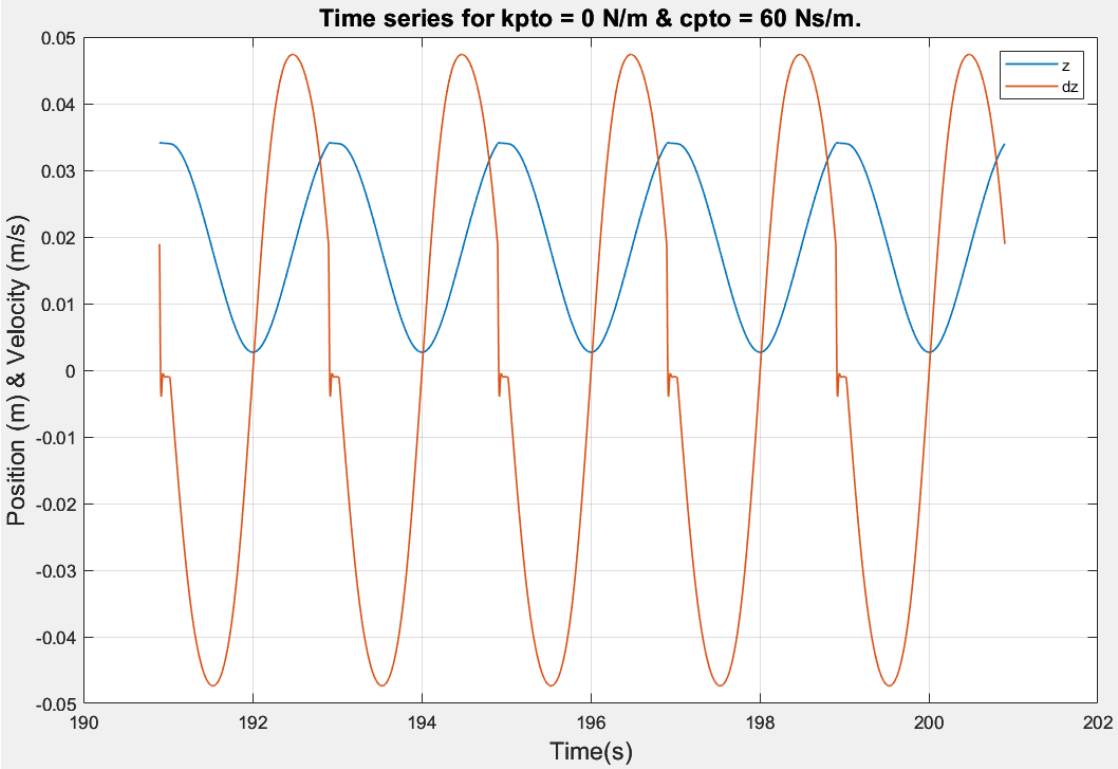

Average power: 0.0729 W

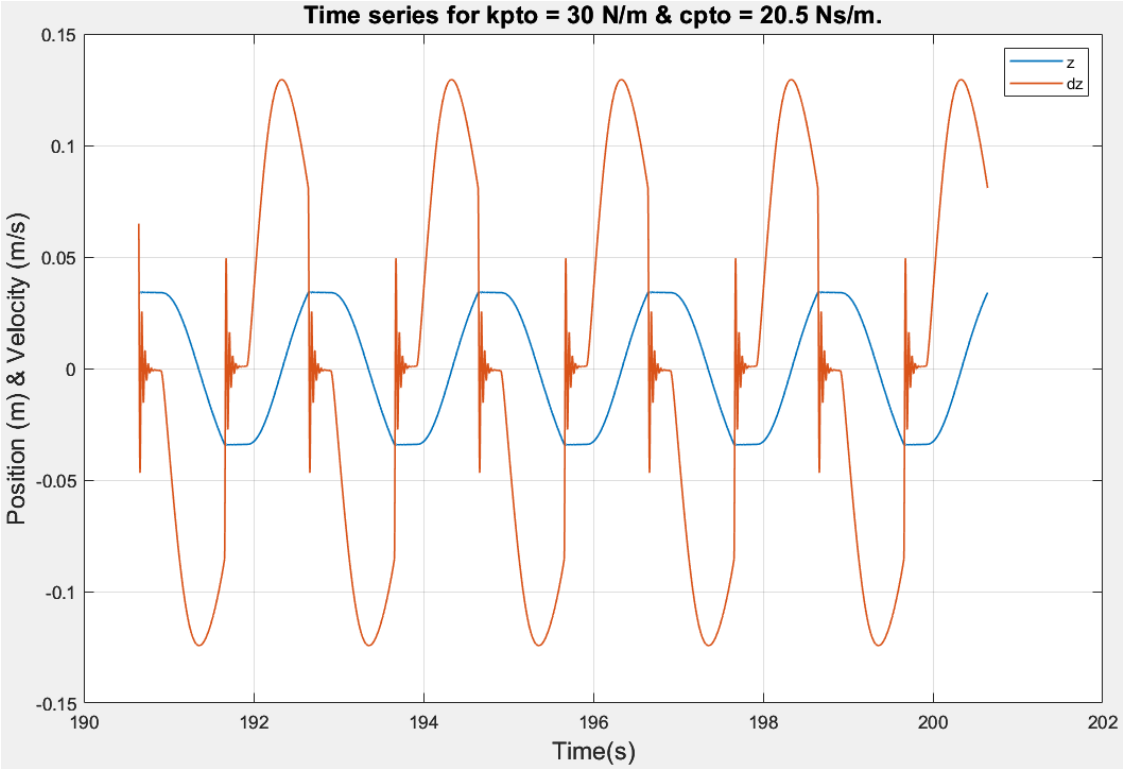

Average power: 0.1497 W

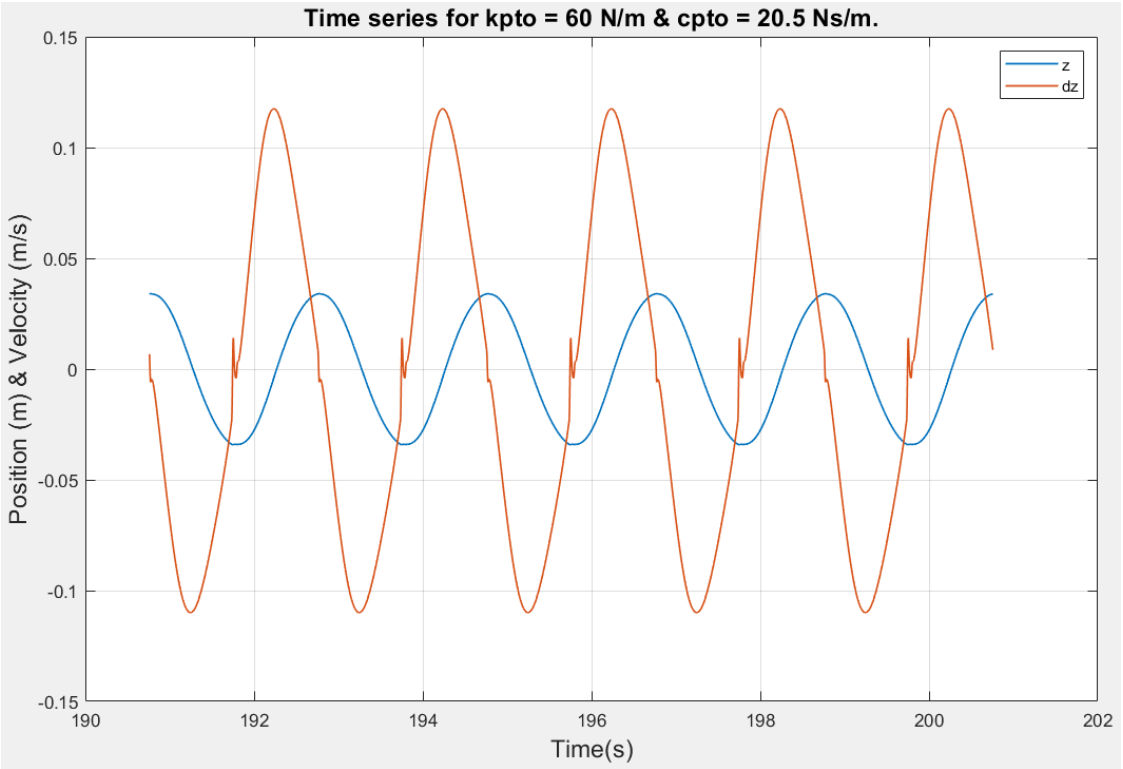

Average power: 0.1216 W

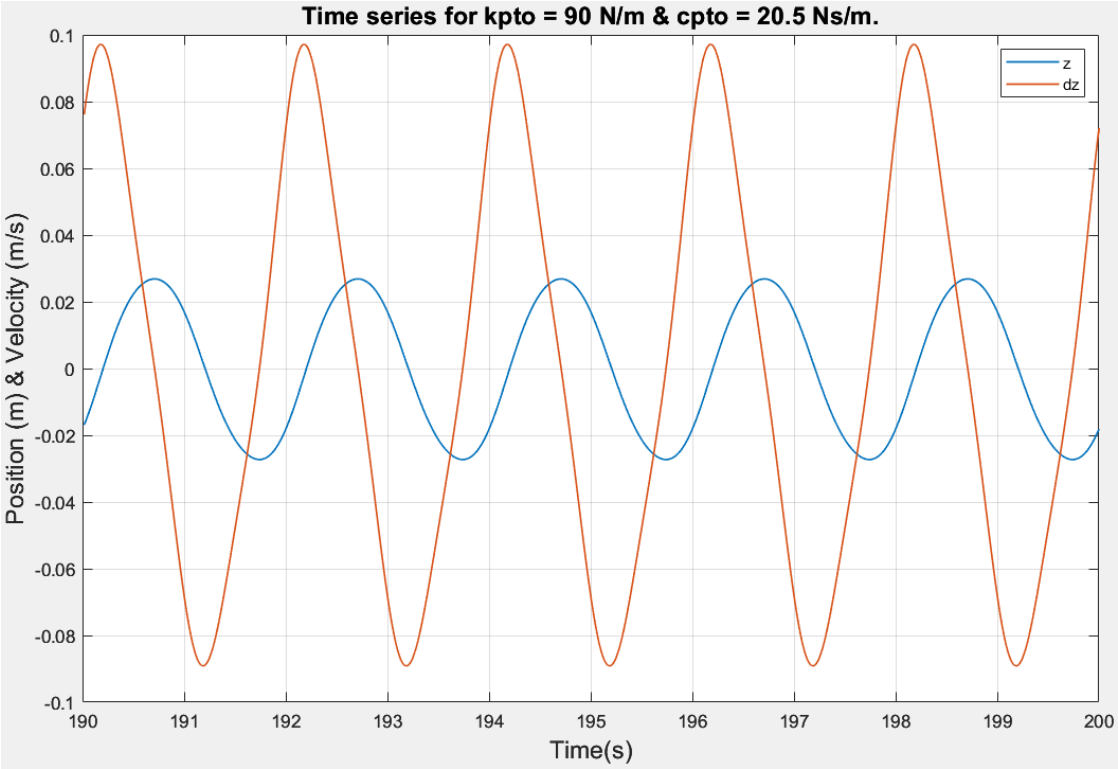

Average power: 0.0778 W

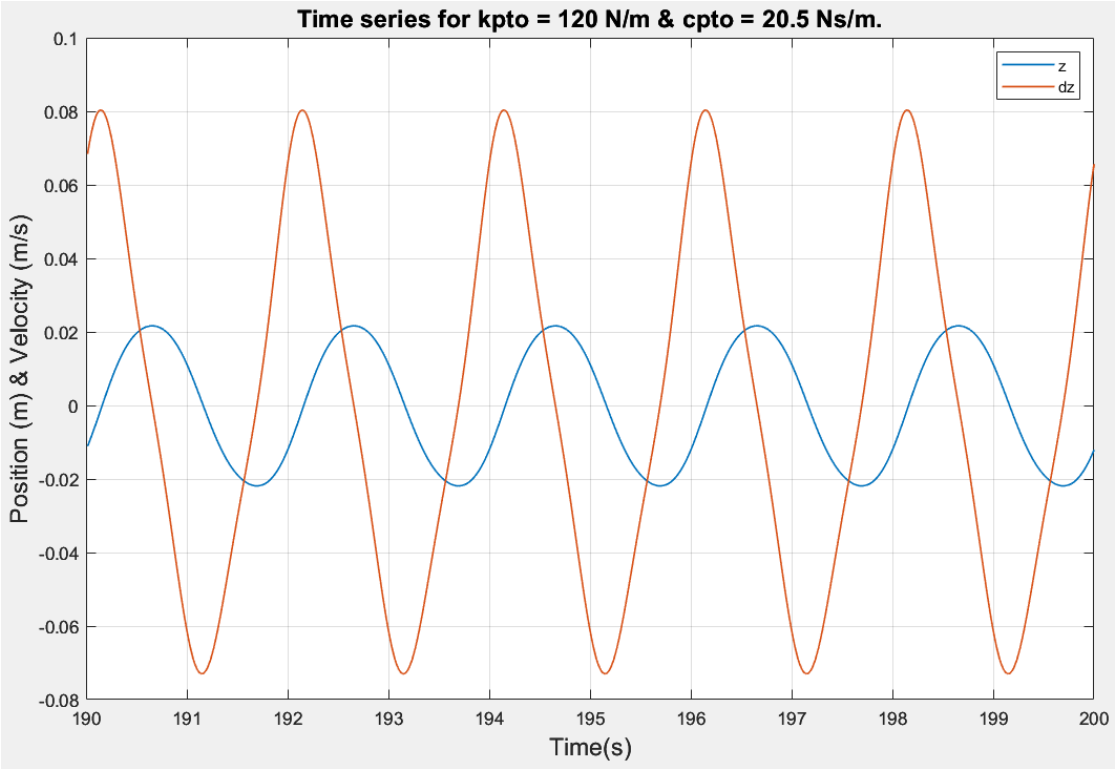

Average power: 0.0511 W

Fig. 19. Position-velocity-time plots for a wave of frequency 0.5 Hz and height 0.113 m.

Results Analysis

The experimental campaign has been done in two stages. In the first stage, the AUV model was mounted on an experimental test rig to perform dry testing. The translation of the oscillating AUV mass with sinusoidal servo motor motion was observed. Different combination of mass, spring constant, and damping coefficient has been explored. However, preliminary testing showed that the generated damping is not enough to observe the behavior or power extraction. So, for wave tank testing, the PTO was set fixed and the AUV model movement in waves were analyzed.

The converter behavior was observed for both vertical and horizontal orientation in four different wave frequency and amplitude configurations. The representative time lapse motion for one complete oscillation of the sealed PTO system is shown in Figure 12 & 13 for vertical orientation and in 14 & 15 for horizontal orientation. The motion obliges the theoretical prediction made by (Yang & Martinez, 2023). Comparing the figures, it can be said that, in vertical orientation the model oscillation amplitude is significantly higher than that in horizontal configuration.

The numerical simulation has also been done for both vertical and horizontal orientation. Table 2 shows the simulation parameters. The absorbed power for different wave frequency and amplitude is calculated for different spring constant, k_{PTO} and damping coefficient C_{PTO}. The maximum absorbed power increases with wave frequency and amplitude. This is the case for both orientations, as shown in Figure 16 & 18. For vertical orientation, maximum power is absorbed for a substantial value of k_{PTO}. But for horizontal orientation maximum power is absorbed when there is no spring constant or without a spring. This can be visualized because for vertical orientation the mass oscillates as the spring pushes it from bottom. But for horizontal orientation

or surface riding configuration, the mass moves due to gravitational force. Hence, without a spring, the translation increases.

Position-velocity-time plots for different combination of k_{PTO} and C_{PTO} is shown in Figure 17 & 19 for vertical and horizontal orientation, respectively. The z and dz lines of the figure illustrate the position and velocity of the oscillating mass respectively.

From numerical simulation we can see that for the same AUV amplitude, the horizontal orientation absorbs almost twice as energy as vertical. However, achieving the same AUV amplitude as vertical orientation is difficult for horizontal case, which is apparent from experimental observation. Moreover, in horizontal orientation, the AUV needs to be aligned with the ocean wave to achieve a good energy absorption. This is quite impossible considering the complex and nonlinear ocean environment. On the other hand, vertical orientation does not have such requirement. So, considering all the factors, from the next section experimental and numerical work has only been done for the vertical orientation.

CHAPTER IV

ANALYSIS OF A BIG-SCALE PTO MODEL

3D Modeling of the Designed 1:3 Scale PTO System

The 3D model of the 1:3 scaled PTO system is shown in Figure 20. The working principle and PTO system of the model is similar to the previous 1:5 scaled model. The modification in design is made based on the issues faced and experience gathered during the machining, assembly, and experimental testing stages. The most severe problem encountered was the inadequate damping force created by the pneumatic damper. To increase the damping, two modifications have been done. To increase the compressed air volume, the solid damper rod has been replaced with a hollow one. The thickness of the damper house cylinder has been reduced to allow more air inside. The second modification is that the diameter of the oscillating center mass has been increased to a value close to the inside diameter of the outer hull. This modification is done to create an additional damping due to the compression of the air inside the cylinder by the oscillating mass.

The next critical issue is the alignment issue. The mass connected with the damper rod needs to be perfectly aligned with the damper tube for smooth oscillation. One single damper rod has been used to attach with the mass and spring pins have been applied to hold the total oscillating mass system together. In this way, the alignment issue can be easily circumvented. Between the

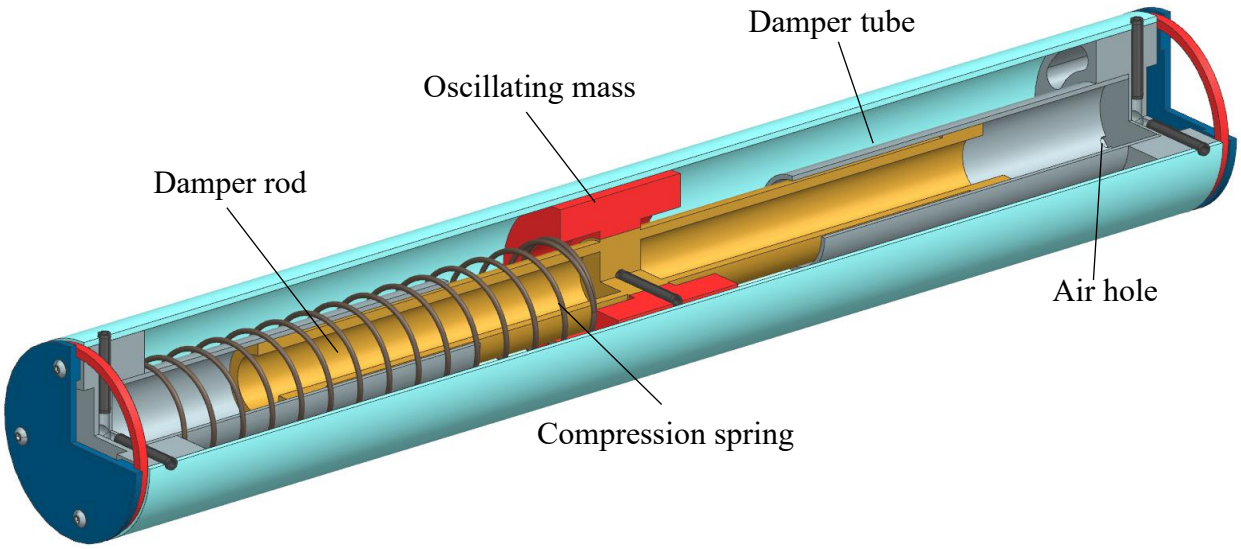

Fig. 20. 3D model of the 1:3 scaled sealed PTO system.

outer hull and the end cap oil rings of rectangular cross section have been used. These would provide an alternative means to achieve good alignment and a flat surface for the end cap to sit on.

In this design compression spring has been used in one side of the oscillating mass similar to the Figure 4. The plan is to deploy this model in vertical orientation (Figure 6) while the spring pushes the mass upward from the bottom. The stiffness of the spring should be enough to hold the oscillating mass 0.1" above the end point at the extreme stroke. This would protect the structure from damage by implementing an end constraint. The whole structure is designed to be watertight to keep the inside parts corrosion free.

The Physical Model and Prototype Configurations

Based on the 3D design, a 1:3 sealed PTO system was fabricated. The individual parts of the PTO system were machined in the UTRGV machine shops using appropriate machine tools by the author and the assigned senior design team. The prototype parts were fabricated keeping in

mind the dry experimental rig and wave tank testing. Several changes were made to the original 3D design depending on the machining complexity, assembly issues, and testing requirements.

The individual parts and the total assembly of the 1:3 scaled model is shown in Figure 21.

(a) (b) (c) (d)

Fig. 21. 1:3 scaled model; (a) PTO mass, (b) damper house, (c) outer hull, (d) the assembled model.

The oscillating center mass is connected with the damper rod with the help of a spring pin. In the original 3D design, only one spring pushes the mass from the bottom. But in the physical model, an expansion spring is also used, besides the compression spring. The expansion spring pulls the mass from the top to add more force to the mass. This modification was done to levitate the mass 0.1 inch from the bottom end as the compression spring was not strong enough. Besides this, 3D-printed plastic end caps have been used in case of wave tank testing to create better sealing.

Dry Test of the 1:3 Scaled Model

The dry testing aimed to identify the damping coefficient of the physical model. This identification was performed by comparing the dry testing result with the numerical result. The maximum displacement of the oscillating mass was chosen as the performance-measuring parameter. Servo motor sinusoidal motion frequency and amplitude were varied for different airhole diameters. The experimental setup is shown in Figure 22.

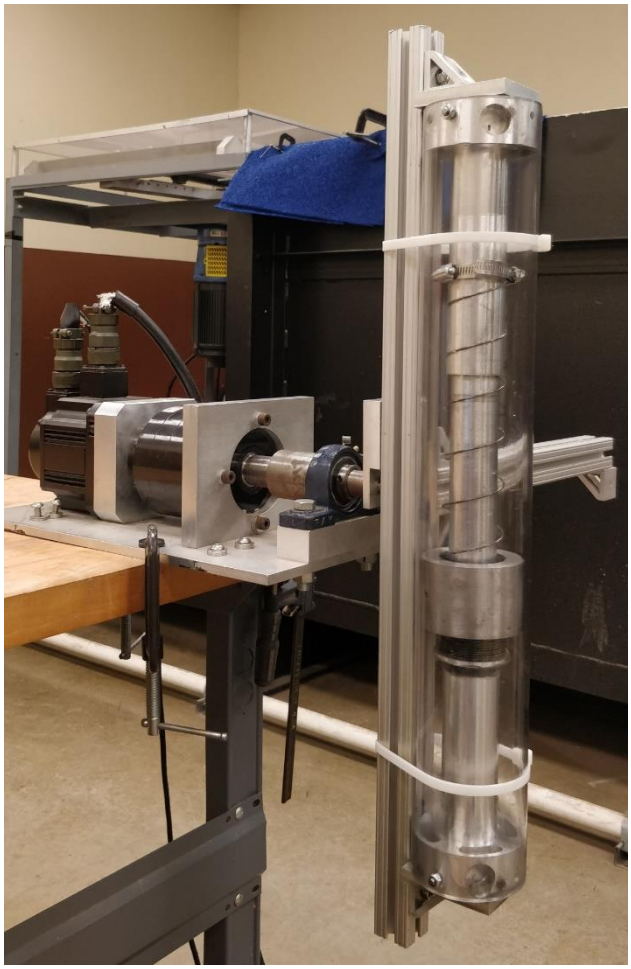

Fig. 22. 1:3 scaled model mounted on experimental dry test rig.

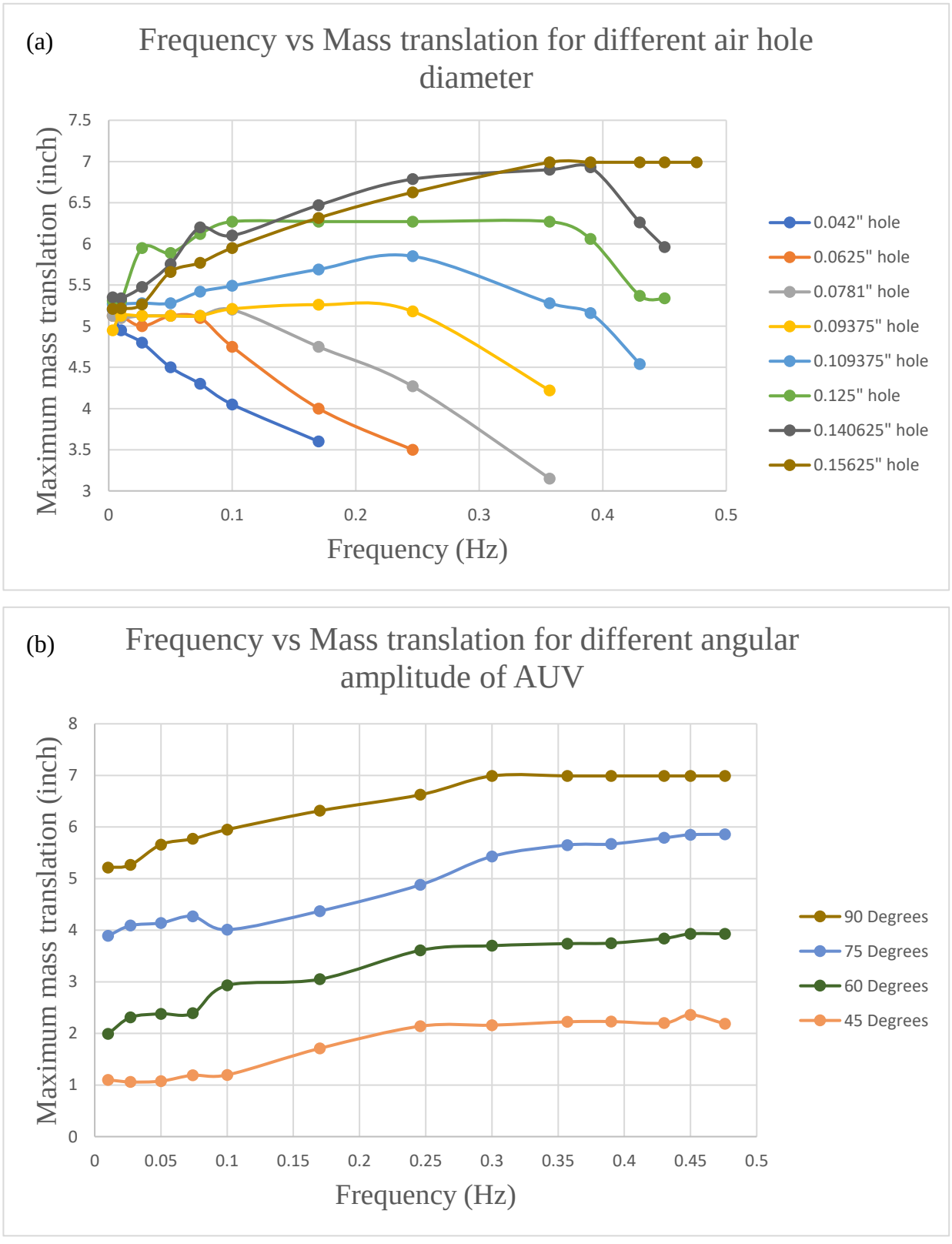

Fig. 23. Frequency and mass translation for; (a) different air hole diameters, and (b) different AUV amplitude.

At first, the airhole diameter was calibrated to obtain a steady high displacement for the mass. Different airhole diameters from 0.042-0.15625 inches were tried for a frequency range of 0-0.5 Hz. The amplitude of oscillation was taken to be 90 degrees both ways. The frequency vs oscillating mass displacement for different airhole diameters is shown in Figure 23(a). The displacement plot shows similar trends for all the airhole diameters that guarantee the prototype's stability and repeatability. The same tendency can also be seen for different motor amplitudes (Figure 23(b)). Finally, an airhole diameter of 0.15625 inches has been chosen as the final dimension because of a steady 7-inch mass displacement up to 0.5 Hz frequency.

Numerical Simulation of the 1:3 Scaled Model

Numerical simulation of the oscillating mass motion is performed for a range of servo motor frequencies and amplitudes. Equations 1-3 have been used for the simulation. The centrifugal force component for heave is discarded for the simulation as this motion is not created in dry test. The numerical simulation aimed to obtain the comparison data for the dry test. The simulation parameters are documented in Table 2. The maximum displacement for 60 and 90 degrees AUV amplitude is obtained to compare with the dry test results. The frequency is varied from 0.1-0.5 Hz frequency. From the comparison, the prototype damping coefficient was tried to identify.

Table 2: Simulation parameters of the 1:3 scaled model.

Simulation Parameters	1:3 Scaled Model
Oscillating mass, m (kg)	2.98
Half of total sliding length, z_0 (m)	0.09
Servo motor frequency, f_W (Hz)	0.1-0.5
Spring constant, k_{PTO} (N/m)	179
Damping coefficient, C_{PTO} (Ns/m)	0-50
Disk spring constant, n	0
Angular oscillation amplitude, θ_0	$\frac{\pi}{3}°, \frac{\pi}{2}°$
Initial phase angle, ϕ_0	0°
Static equilibrium constant, ε	-1
Initial condition, i_C	$z_{PTO} = 0, \frac{dz_{PTO}}{dt} = 0$

Analysis of the Dry Test and Numerical Simulation

Under the two angular amplitudes, as shown in Figure 23, in a low frequency range the numerical results match well with the experimental. However, in a high frequency range, the damping behavior is much more complex. In the low frequency range, the mechanical friction is relatively strong compared to the air damping. Hence, the displacement is quite similar for a large damping range. On the other hand, the damping behavior dominates in a high frequency. It is possible to match the experimental damping value with a numerical run at a specific AUV

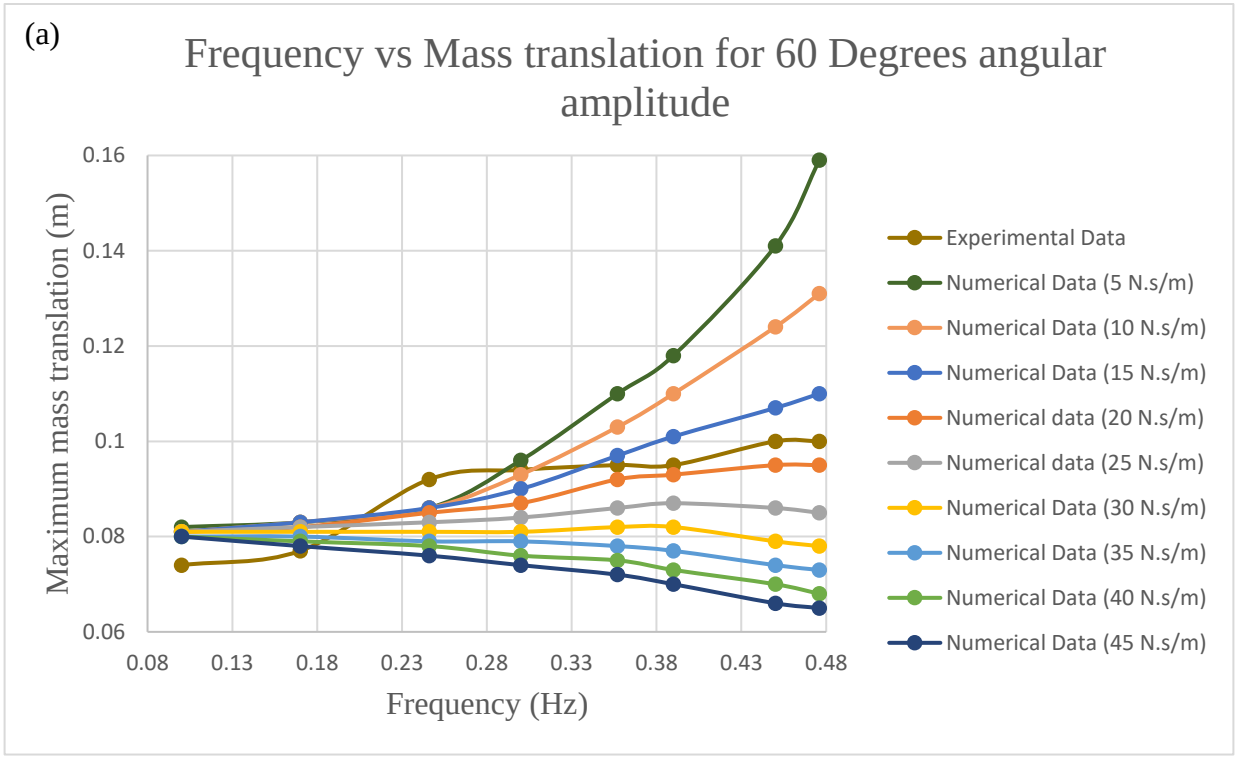

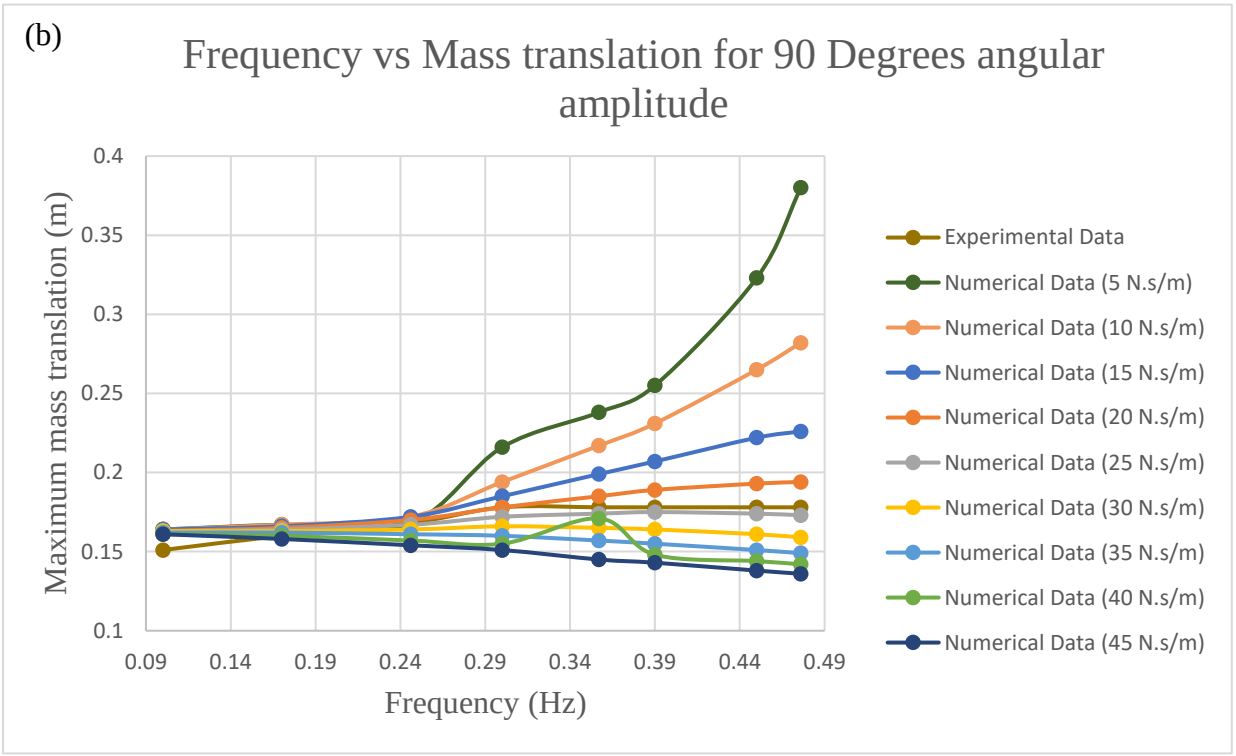

Fig. 24. Frequency and mass translation for; (a) 60, and (b) 90 Degrees of AUV angular amplitude.

amplitude (20 N.s/m for 60 degrees and 25 N.s/m for 90 degrees), but for different angular amplitudes the matched damping coefficients are different. Due to this, for future research, we will only focus on the high frequency range (e.g., f_W >= 0.3 Hz), and try to assume a constant damping coefficient to identify a relatively reasonable match between the experimental and numerical results.

Wave Tank Testing

The wave tank testing on the large-scale model was done to see its performance in actual working environment. It was made sure that no water leaked into the model. Silicon sealant was used for this purpose. Four different wave frequencies (0.3,0.5,0.6,07) and amplitudes (0.137, 0.113, 0.198, 0.242) combinations were tested. The AUV mass movement was very minimal for all the frequency-amplitude combination. The dominating reason behind that is the inadequate pitching motion of the AUV model.

Two solutions in consideration to improve the pitch resonance of the AUV model in ocean waves. First, to decrease the submergence of the model and second, to use a passive flow control technique such as fins. The synchronization between the AUV model and ocean waves can be improved by decreasing the AUV submersion. The stability of the model needs to be lessened to increase the pitch amplitude. To decrease the submergence, the oscillating mass was reduced.

A passive control technique using fins can increase wave resistance while the waves pass through the prototype. There will be a propeller in the actual AUV design, as shown in Figure 26. This will also add to the drag produced by the model. The testing is ongoing now.

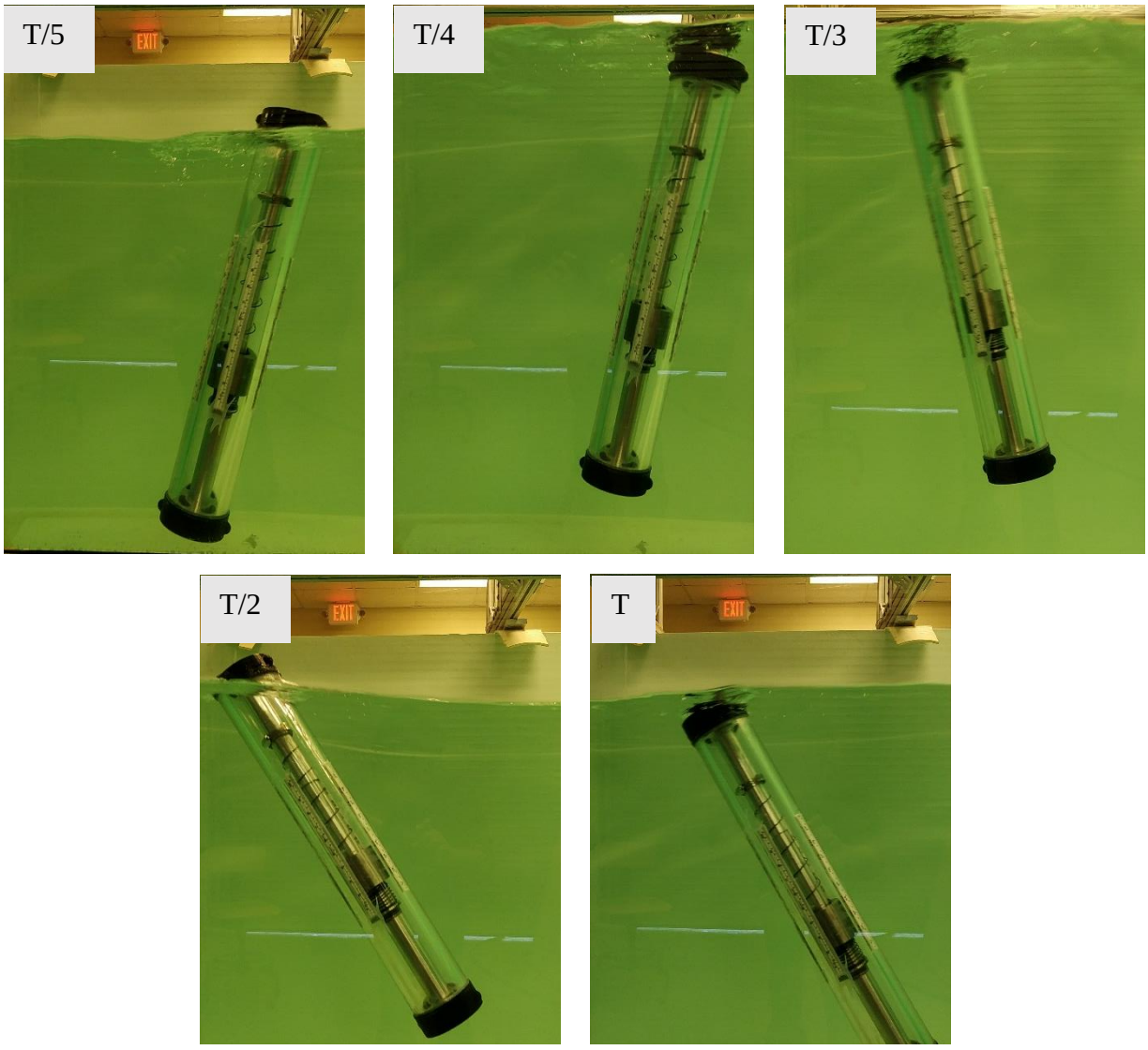

Fig. 25. AUV motion in wave frequency 0.5 Hz and height 0.113 m. Here, T means the wave period.

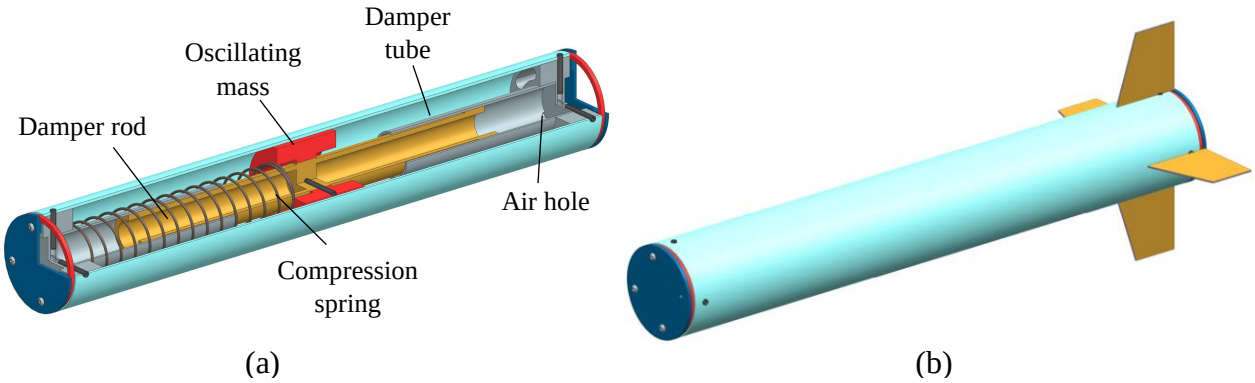

Fig. 26: a) 3D model of the PTO system, b) physical model of the PTO system in wave tank, and c) sealed PTO system with attached fins.

CHAPTER V

CONCLUSION AND FUTURE WORK

Worldwide increasing energy consumption is depleting fossil fuel resources rapidly. Fossil fuel is also the primary culprit for global warming. But thanks to renewable energy, there is still hope. Ocean wave belongs to the marine renewable energy category and has significant advantages over other counterparts. Wave energy converter development has a long history and more than 1,000 WEC designs of different types have been proposed globally. But still, the technology lags far behind solar and wind in terms of maturity. The reason behind this is the unpredictable nature of the oscillating wave motion. Marine life and extreme wave conditions add salt to the injury.

One of the possible applications of ocean waves is powering autonomous underwater vehicles (AUVs). Several researchers have tried to incorporate marine renewable energy (e.g., solar, wind, ocean thermal) into the AUVs. But none has met the expectation yet. In this thesis, a wave energy powered AUV concept has been proposed. The permanent magnet linear generator (PMLG) PTO of the self-powered AUV is designed as a mass-spring damper system. The PTO and other mechanical and electrical components are sealed inside a rigid hull to prevent corrosion.

The detailed concept of the self-recharging AUV and its motion in waves is described. A mathematical model of the mass translation in AUV for both vertical and horizontal orientation is formulated considering heave and pitch motion.

The first stage of research began with modeling and prototyping a 1:5 scaled sealed PTO system. An experimental test rig was developed for preliminary dry testing of the prototype. The converter performance was not satisfactory. The generated damping was not strong enough to show any significant energy conversion. However, the wave tank testing with fixed PTO showed inspiring motion. The numerical and experimental analysis confirmed the superiority of vertical orientation over horizontal.

Based on the experience gathered in the first-generation prototype, a modified 1:3 large-scale PTO system was proposed. The improvements were focused on increasing the prototype damping. Extensive dry testing has been done on the second-generation model. The new model showed excellent performance in dry testing. A suitable damping was chosen by tuning the model. PTO mass displacement was taken as the performance parameter. Comparison between numerical and experimental result showed that the maximum displacement values are almost identical for low frequencies. However, in high frequency, the damping behavior is much more complex. In the last stage, the converter behavior in waves was analyzed. The PTO mass displacement was minimal because of the weak pitch amplitude of the prototype.

Future research should focus on tuning the sealed PTO system to generate strong pitch motion in waves. Moreover, the damping behavior of the model in high frequency needs to be analyzed. This is required to identify the damping constant of the prototype. Finally, a more sophisticated numerical model needs to be developed to understand the wave hydrodynamic effects on AUV.

REFERENCES

Aderinto, T. & Li, H. (2018). Ocean Wave Energy Converters: Status and Challenges. *Energies,* 11, 1250.

Ageev, M. D., & Blidberg, D. R. (2002). Current Progress in the Development of a Solar Powered Autonomous Underwater Vehicle (AUV). *In: Proceedings of 1998 International Symposium on Underwater Technology*.

Aguirre, F., Vargas, S., Valdés, D., & Tornero, J. (2017). State of the Art of Parameters for Mechanical Design of an Autonomous Underwater Vehicle. *International Journal of Oceans and Oceanography,* 11(1), 89-103.

Ahn, S., Haas, K. A., & Neary, V. S. (2021). Wave energy resource characterization and assessment for coastal waters of the United States. *Applied Energy,* 267, 114922.

Ahn, S., Neary, V. S., Allahdadi, M. N., & He, R. (2021). Nearshore wave energy resource characterization along the East Coast of the United States. *Renewable Energy,* 172, 1212-1224.

Astariz, S., & Iglesias, G. (2015). The economics of wave energy: A review. *Renewable and Sustainable Energy Reviews,* 45, 397-408.

Astariz, S., & Iglesias, G. (2015). Wave energy vs. other energy sources: A reassessment of the economics. *International Journal of Green Energy,* 13(7), 747-755.

Basañez, A., & Pérez-Muñuzuri, V. (2021). HF Radars for Wave Energy Resource Assessment Offshore NW Spain. *Remote Sensing,* 13, 2070.

Blidberg, D., Mupparapu, S., Chappell, S., & Komerska, R. (2005). The SAUV ll (Solar Powered AUV) Test Results 2004. *In: Europe Oceans 2005*.

Borthwick, A. G. L. (2016). Marine Renewable Energy Seascape. *Engineering,* 2, 69-78.

BP (2021). *Statistical Review of World Energy: 70th edition.* London, UK: BP.

Budar, K. & Falnes, J. (1974). A resonant point absorber of ocean-wave power. *Nature,* 256.

Chen, Z., Zhou, B., Zhang, L., Sun, L., & Zhang, X. (2018). Performance evaluation of a dual resonance wave-energy converter in irregular waves. *Applied Ocean Research,* 77, 78-88.

Clément, A., McCullen, P., Falcão, A., Fiorentino, A., Gardner, F., Hammarlund, K. et al. (2002). Wave energy in Europe: current status and perspectives. *Renewable and Sustainable Energy Reviews,* 6, 405-431.

Colton, W. (2013). *The Outlook for Energy: A View to 2040.* Singapore: ExxonMobil.

Crimmins, D. M., Patty, C. T., Beliard, M. A., Baker, J., Jalbert, J. C., Komerska, R. J., et al. (2006). Long-Endurance Test Results of the Solar-Powered AUV System. *In: Oceans 2006*.

Cruz, J. (2008). *Ocean Wave Energy: Current Status and Future Perspectives.* Heidelberg, Berlin: Springer.

Czech, B. & Bauer, P. (2012). Wave Energy Converter Concepts: Design challenges and classification. *IEEE Industrial Electronics Magazine*, 6, 4–16.

Dresner, S. (2002). *The Principles of Sustainability.* UK: Earthscan.

EC (2019). *Clean energy for all Europeans.* Luxembourg: EU.

Edenhofer, O., Madruga, R. P., Sokona, Y., Seyboth, K., Matschoss, P., Kadner, S., et al. (2012). *Renewable Energy Sources and Climate Change Mitigation: Special Report of the Intergovernmental Panel on Climate Change.* NY, USA: Cambridge University Press.

EMEC: The European Marine Energy Center LTD. Wave devices, https://www.emec.org.uk/marine-energy/wave-devices/; 2022 [accessed 19 April 2023].

Ermakov, A. & Ringwood, J. V. (2021). Rotors for wave energy conversion—Practice and possibilities. *IET Renewable Power Generation,* 15, 3091-3108.

Evans, D. V. (1976). A theory for wave-power absorption by oscillating bodies. *Journal of Fluid Mechanics*, 7, 1–25.

Falcão, A. F. de O. (2010). Wave energy utilization: A review of the technologies. *Renewable and Sustainable Energy Reviews,* 14, 899-918.

Falnes, J. (2007). A review of wave-energy extraction. *Marine Structures*, 20, 185-201.

Falnes, J. (1993). Optimum Control of Oscillation of Wave-energy Converters. *In: The eleventh International Offshore and Polar Engineering Conference.*

Gao, Y., Shao, S., Zou, H., Tang, M., Xu, H., & Tian, C. (2016). A fully floating system for a wave energy converter with direct-driven linear generator. *Energy*, 95, 99-109.

Goharnejad, H., Nikaein, E, & Perrie, W. (2021). Assessment of wave energy in the Persian Gulf: An evaluation of the impacts of climate change. *Oceanologia, 63*, 27-39.

Grilli, A. R., Merrill, J., Grilli, S.T., Spaulding, M. L., & Cheung, J. T. (2007). Experimental and Numerical Study of Spar Buoy-magnet/spring Oscillators Used as Wave Energy Absorbers. *In: Proceedings of the Seventeenth International Offshore and Polar Engineering Conference.*

Henry, A., Rafiee, A., Schmitt, P., Dias, F., & Whittaker, T. (2014). The Characteristics of Wave Impacts on an Oscillating Wave Surge Converter. *Journal of Ocean and Wind Energy*, 1(2), 101-110.

Hernandez-Sanchez, T., Bonasia, R, & Scaini, C. (2021). Feasibility Study for the Extraction of Wave Energy along the Coast of Ensenada, Baja California, Mexico. *Journal of Marine Science and Engineering*, 9, 284.

IEA (2020). *Energy Technology Perspective.* IEA.

IEA (2015). *World Energy Outlook.* Paris, France: IEA.

IEA, IRENA, UN, WB, and WHO. (2020). *Tracking SDG 7: The Energy Progress Report.* Washington, DC: The World Bank.

Ilyas, A., Kashif, S. A. R., Saqib, M. A., & Asad, M. A. (2014). Wave electrical energy systems: Implementation, challenges and environmental issues. *Renewable and Sustainable Energy Reviews,* 40, 260-268.

IRENA (2014). *Wave Energy Technology Brief.* IRENA.

Inger, R., Attrill, M. J., Bearhop, S., Broderick, A. C., Grecian, W. J., Hodgson, D. J., et al. (2009). Marine renewable energy: potential benefits to biodiversity? An urgent call for research. *Journal of Applied Ecology,* 46, 1145-1153.

Jalbert, J., Baker, J., Duchesney, J., Pietryka, P., Dalton, W., Blidberg, D. R., et al. (2004). A Solar-powered Autonomous Underwater Vehicle. *In: Europe Oceans 2005*.

Komerska, R. J., & Chappell, S. G. (2006). A Simulation Environment for Testing and Evaluating Multiple Cooperating Solar-powered AUVs. *In: Oceans 2006*.

Lacal-Arantegui, R., Jäger-Waldau, A., Vellei, M., Sigfusson, B., Magagna, D., Jakubcionis, M., et al. (2014). *DRAFT 2014 energy technology reference indicator (ETRI) projections for 2010–2050.* Luxembourg: Publications Office of the European Union.

Lindquist, H. (2017). The journey of reinventing the European electricity landscape. *In: Jones LE, editors. Renewable energy integration,* Amsterdam: Elsevier Inc, p 3-13.

López, I., Andreu, J., Ceballos, S., de Alegría, I. M. & Kortabarria, I. (2013). Review of wave energy technologies and the necessary power-equipment. *Renewable and Sustainable Energy Reviews,* 27, 413-434.

Masuda, Y. (1986). An experience of wave power generator through tests and improvement. *In: Hydrodynamics of Ocean Wave-Energy Utilization.* Berlin: Springer, p. 445–52.

Mayer, A. (2019). Partisanship, politics, and the energy transition in the United States: A critical review and conceptual framework. *Energy Research & Social Science,* 53, 85-88.

Mueller, M., & Wallace, R. (2008). Enabling science and technology for marine renewable energy. *Energy Policy,* 36, 4376-4382.

Nikolkina, I., & Didenkulova, I. (2011). Rogue waves in 2006–2010. *Natural Hazards and Earth System Sciences,* 11, 2913-2924.

O'Brien, L., Dudley, J. M., & Dias, F. (2013). Extreme wave events in Ireland: 14 680 BP–2012. *Natural Hazards and Earth System Sciences,* 13, 625-648.

Pecher, A. & Kofoed, J. P. (2017). *Handbook of Ocean Wave Energy.* Switzerland: Springer.

Pelc, R., & Fujita, R. M. (2002). Renewable energy from the ocean. *Marine Policy,* 26, 471-479.

Roberts, G., Sutton, R. (2006*). Advances in Unmanned Marine Vehicles.* London, UK: Institution of Engineering and Technology.

Salter, S. H. (1974). Wave power. *Nature,* 249, 720-724.

Shami, E. A., Zhang, R., & Wang, X. (2018). Point Absorber Wave Energy Harvesters: A Review of Recent Developments. *Energies,* 12, 47.

Sheng, W. (2019). Wave energy conversion and hydrodynamics modelling technologies: A review. *Renewable and Sustainable Energy Reviews,* 109, 482-498.

Shi, W., Wang, D., Atlar, M., Guo, B., & Kwang-cheol, S. (2015). Optimal design of a thin-wall diffuser for performance improvement of a tidal energy system for an AUV. *Ocean Engineering,* 108, 1-9.

Smith, R. N., & Hyunh, V. T. (2014). Controlling Buoyancy-Driven Profiling Floats for Applications in Ocean Observation. *IEEE Journal of Oceanic Engineering,* 39(3).

Taveira-Pinto, F., Iglesias, G., Rosa-Santos, P., & Deng, Z. D. (2015). Preface to Special Topic: Marine Renewable Energy. *Journal of Renewable and Sustainable Energy,* 7, 061601.

Tiron, R., Mallon, F., Dias, F., & Reynaud, E. G. (2015). The challenging life of wave energy devices at sea: A few points to consider. *Renewable and Sustainable Energy Reviews,* 43, 1263-1272.

Tiron, R., Pinck, C., Reynaud, E. G., & Dias, F. (2012). Is Biofouling a Critical Issue for Wave Energy Converters? *In: Twenty-second International Offshore and Polar Engineering Conference (ISOPE)*, p. 669–79.

Topper, M. B. R., Nava, V., Collin, A. J., Bould, D., Ferri, F., Olson, S. S., et al. (2019). Reducing variability in the cost of energy of ocean energy arrays. *Renewable and Sustainable Energy Reviews,* 112, 263-279.

Townsend, N. C. (2016). Self-powered autonomous underwater vehicles: results from a gyroscopic energy scavenging prototype. *IET Renewable Power Generation,* 10(8), 1078-1086.

Townsend, N. C., & Shenoi, R. A. (2016). Feasibility study of a new energy scavenging system for an autonomous underwater vehicle. *Auton Robot,* 40, 973-985.

Uihlein, A., & Magagna, D. (2016). Wave and tidal current energy – A review of the current state of research beyond technology. *Renewable and Sustainable Energy Reviews,* 58, 1070-1081.

UN (2015). *Adoption of the Paris Agreement.* United Nations.

UN (2017). *The Ocean Conference.* NY: United Nations.

Xu, J., Shi, J., & Zhang, C. (2020). Wave energy assessment along Chinese coasts based on a 40-year hindcast. *In: Proceedings of the 3rd International Conference on Sustainability in Civil Engineering (ICSCE).* Singapore; Springer, p. 295–301.

Yang, Y., Jenet, F., Xu, B., Garza, J. C., Tamayo, B., Chavez, Y., et al. (2019). Experimental Study of a Lift-Type Wave Energy Converter Rotor in a Freewheeling Mode. *Journal of Energy Resource and Technology,* 142, 031201-1.

Yang, Y., & Martinez, E. (2023). Feasibility analysis of a wave powered autonomous underwater vehicle. *Energy Conversion and Management: X*, 18, 100352.

Zhang, Y., Zhao, Y., Sun, W., & Li, J. (2021). Ocean wave energy converters: Technical principle, device realization, and performance evaluation. *Renewable and Sustainable Energy Reviews*, 141, 110764.

BIOGRAPHICAL SKETCH

Mahmodul Hasan Maheen earned a Bachelor of Science (B.Sc.) in Mechanical Engineering from Bangladesh University of Engineering and Technology (BUET). He worked as a lecturer in the textile engineering department of Daffodil International University, Dhaka. In January 2021, he resumed his graduate studies in Department of Mechanical Engineering at the University of Texas Rio Grande Valley (UTRGV), with the goal of earning a master's degree. Mahmodul began his study at UTRGV, where he was supervised by Dr. Yingchen Yang, Professor. He has been given the Presidential Graduate Research Assistantship (PGRA). He was assigned a year of Graduate Research Assistantship and a year of Graduate Teaching Assistantship. Maheen earned a Master's degree in Mechanical Engineering in May 2023. He intends to pursue a Ph.D. in any prestigious school or institution in the United States and do research on Ocean Engineering field. Contact information for Mahmodul Hasan Maheen: mahmodulhasanmaheen@gmail.com.